Numerical Upper and Lower Bound Limit Analysis for Braced Excavations

by

Fernando G. Degwitz

B.S. Civil and Environmental Engineering
Tufts University, 2003

SUBMITTED TO THE DEPARTMENT OF CIVIL AND ENVIRONMENTAL ENGINEERING IN PARTIAL COMPLETION OF THE REQUIREMENTS FOR THE DEGREE OF

MASTER OF ENGINEERING IN CIVIL AND ENVIRONMENTAL ENGINEERING
AT THE
MASSACHUSETTS INSTITUTE OF TECHNOLOGY

JUNE 2004

Signature of Author:.....
Department of Civil and Environmental Engineering
May 7, 2004

Certified by:.....
Andrew J. Whittle
Professor of Civil and Environmental Engineering
Thesis Supervisor

Accepted by:.....
Heidi Nepf
Chairman, Departmental Committee on Graduate Students

Numerical Upper and Lower Bound Limit Analysis for Braced Excavations

by

Fernando G. Degwitz

Submitted to the Department of Civil and Environmental Engineering
on May 7th, 2004 in Partial Fulfillment of the Requirements for the
Degree of Master of Engineering in Civil and Environmental Engineering

Abstract

This thesis reviews limit theorems and their applications for stability problems in geotechnical engineering.

Rigorous numerical solutions of limit analyses can be obtained through finite element discretization of the soil mass and formulation of the limit theorems within a linear programming framework. The current research uses a formulation proposed by Sloan et al. (1988) and extended in a recent Ph.D. thesis by Ukritchon (1998) to include soil-structure interactions.

The thesis details the input and output required for numerical limit analysis and presents an example application for the stability of a broad excavation for the MUNI Metro Turnback project in San Francisco. This well documented case study involves a 13 M deep excavation within a deep deposit of May Mud that was supported by an SPTC wall with three levels of cross-lot bracing. The numerical limit analyses calculate factors of safety, FS = 1.03 – 1.36, against basal instability. The factor of safety used in the original design (FS = 1.2) is contained in this range. The results illustrate that numerical limit analysis offers a practical alternative to limit equilibrium methods in evaluating the stability of braced excavations.

Thesis Supervisor: Andrew Whittle
Title: Professor of Civil and Environmental Engineering

Dedication

To my family.

Acknowledgements

I would like to take this opportunity to thank a few people who made this thesis possible and bearable.

Professor Whittle, Thesis Supervisor. If you have ever been to Professor Whittle's office, you know there is *always* a line of students who want to speak to Professor Whittle, and somehow he always had time for each one.

MIT, for letting me do the one thing I remember always wanting to do: earn my Brass Rat.

Chagu, for his support throughout the thesis process despite the fact I did not have time to talk to him often.

Manuela Barreto, because even people who think they are self-motivated sometimes need motivation.

The Course 1 M. Eng. 2004 group, because they all know by now that I sing while I work, and I am still alive.

To my family, because I would not have made it very far without them.

Table of Contents

Chapter 1. Introduction

Upper and lower bound limit theorems are fundamental principles of plasticity that provide a means to estimate collapse loads for materials that exhibit rigid-perfectly plastic behavior by bounding the exact collapse load (Drucker et al., 1952). The lower bound theorem leads to a lower bound estimate of collapse by considering a statically admissible stress field, where stresses are in equilibrium and do not exceed yield criteria anywhere, and where stress boundary conditions are satisfied. The upper bound theorem leads to an upper bound estimate of collapse by considering a kinematically admissible velocity field, where displacements and velocities satisfy the plastic flow rule, and velocity boundary conditions are satisfied. Statically and kinematically admissible conditions will be discussed in more detail in the following chapters.

Atkinson (1978) explains the principles behind the limit theorems concisely as follows:

"If there is a set of external loads which are in equilibrium with a state of stress which nowhere exceeds the failure criterion for the material, collapse *cannot* occur and the external loads are a lower bound to the true collapse loads."

"If there is a set of external loads and a mechanism of plastic collapse such that the increment of work done by the external loads in an increment of displacement equals the work done by the internal stresses, collapse *must* occur and the external loads are an upper bound to the true collapse loads."

These two principles have numerous beneficial implications for geotechnical engineers. Their first major benefit is their simplicity. Finding a complete solution for failure of a geotechnical engineering problem involves solving the complete field equations (i.e. equilibrium, kinematics, and constitutive behavior) using a constitutive model that can represent the non-linear stress-strain-strength behavior of soils. As opposed to many practical structural engineering problems where elements can often be simplified to one dimension, even the simplest geotechnical engineering problems are multi-dimensional (2D or 3D), with shear strength properties that depend on confining pressure and density. This difficulty often makes these theoretically complete solutions impractical, thus forcing engineers to make simplifications to be able to estimate collapse

loads. Indeed, approximate limit equilibrium methods are widely used in geotechnical practice, although the accuracy of these methods is often unknown.

The simplicity of limit theorems allows the engineer to circumvent the difficulty of these problems. Limit theorems require only the shear strength criterion (as opposed to the complete stress-strain behavior). This makes the problem significantly easier to solve. Moreover, the resulting lower and upper bounds provide the engineer with a built-in check on the accuracy of the collapse load from the computed range between the lower and upper bound loads. Furthermore, the simplifications that are required to apply limit theorems in the context discussed in this paper (e.g. finite element discretization and linearization of yield surfaces) are chosen deliberately so they only affect the precision of the results, not their validity.[1]

The purpose of this paper is to introduce limit theorems and their applications to stability problems in geotechnical engineering. The paper develops the required background theory and practical knowledge necessary to analyze the case that is discussed later in the paper.

Chapter 2 discusses the formulation of the limit theorems. The chapter starts by proving both limit theorems, and then focuses on the formulation of limit theorems within a linear programming framework.

Chapter 3 forms the link between limit theorems and their applications to real problems by discussing how to use the programs that solve the linear programming problem.

Chapter 4 is the numerical limit analysis of the MUNI Metro Turnback project in San Francisco. The theory and practical knowledge developed in Chapters 2 and 3 are applied here to an interesting case study of a deep excavation in clay.

Finally, Chapter 5 concludes the paper with the author's conclusions and recommendations. The author discusses the limitations of the limit theorems and their numerical formulations, and makes recommendations so that these limitations can be avoided in the future.

---

[1] For example, the size of the range that bounds the actual solution decreases with increasing mesh fineness. However, a coarse mesh will still produce a range containing the actual solution.

Chapter 2. Formulation of Limit Theorems

2.1 Proof of the Limit Theorems

This section discusses the proofs of the lower and upper bound limit theorems. Both proofs are taken from Atkinson (1978).

2.1.1 The Flow Rule

Tensors of strain increments can be decomposed into tensors of elastic and plastic strain increments by the following equation:

$$d\varepsilon_{ij} = d\varepsilon^{e}{}_{ij} + d\varepsilon^{p}{}_{ij}, \tag{2.1}$$

where the e subscript indicates elastic strain increments, and the p subscript indicates plastic stain increments. Elastic strain increments can be calculated from elastic theory. Plastic strain increments are calculated from the following equation from plasticity theory:

$$d\varepsilon_{ij}{}^{p} = d\lambda P_{ij}, \tag{2.2}$$

where

$d\varepsilon_{ij}^{p}$ is the second order tensor of plastic strain increment,
$d\lambda$ is a scalar that controls the magnitude of plastic strain increments,
and P_{ij} is a second order tensor controlling the direction of plastic strain increments.

A special case of equation 2.2 occurs when the failure criterion serves as a potential for plastic strains, and the plastic strains are normal to the failure criterion. This condition is referred to as associated flow. For this case, equation 2.2 can be rewritten as

$$d\varepsilon_{ij}{}^{p} = d\lambda \frac{\partial F}{\partial \sigma_{ij}}, \tag{2.3}$$

where

F is the failure criterion,
and σ_{ij} is the second order stress tensor.

Substituting equation 2.3 into 2.1 gives

$$d\varepsilon_{ij} = d\varepsilon_{ij}^{\ e} + d\lambda \frac{\partial F}{\partial \sigma_{ij}}. \tag{2.4}$$

For perfectly plastic materials, elastic strains are zero at failure (denoted *f*) and equation 2.4 becomes

$$d\varepsilon_{ij}^{f} = d\lambda \frac{\partial F}{\partial \sigma_{ij}}. \tag{2.5}$$

Therefore, if the flow rule is associated, then incremental postfailure strains of perfectly plastic materials will be normal to the failure criterion. The proofs of the limit theorems require equation 2.5 to hold; therefore, the proofs of the limit theorems assume soils are perfectly plastic and the flow rule is associated.

2.1.2 Proof of Lower Bound Theorem

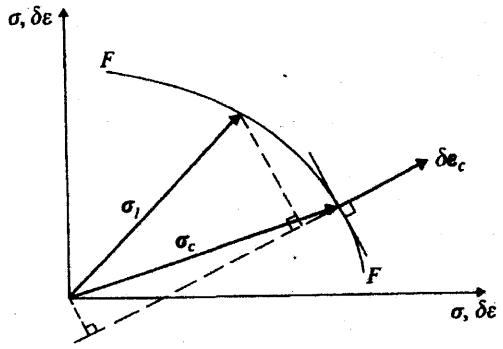

Figure 2.1 Proof of the Lower Bound Theorem (Atkinson and Bransby, 1978).

Figure 2.1 shows a hypothetical failure criterion for a perfectly plastic soil. The subscript *c* indicates the actual stresses and strain increments during collapse, while the subscript *l* indicates the stresses and strain increments corresponding to the lower bound estimates. The σ_c vector corresponds to a stress state on the failure surface, while the σ_l vector lies just inside the failure surface (with an infinitesimally small gap). The plastic strain increment, $\delta\varepsilon_c$, is normal to the failure surface in accordance with the associated flow rule.

The principle of virtual work can be written:

$$\sum F \cdot \delta w = \int_V \sigma \cdot \delta\varepsilon dV, \tag{2.6}$$

where

F is an external force,
δw is the increment of displacement where F is applied,
σ is the internal stress,
and $\delta\varepsilon$ is a strain increment where σ is applied.

The corresponding equation for the exact collapse loads and stresses becomes:

$$\sum F_c \cdot \delta w_c = \int_V \sigma_c \cdot \delta\varepsilon_c dV, \tag{2.7}$$

and the corresponding equation for the lower bound estimate is:

$$\sum F_l \cdot \delta w_c = \int_V \sigma_l \cdot \delta\varepsilon_c dV. \tag{2.8}$$

For simplicity, we can assume $\delta\varepsilon_c$ has a value of unity, and the dot products on the right hand side of equations 2.7 and 2.8 become simply the component of the corresponding stress vector, σ_l or σ_c, in the direction of incremental strain at failure, $\delta\varepsilon_c$, as shown by the constructions in the figure. These constructions reveal that

$$\sigma_l \cdot \delta\varepsilon_c \leq \sigma_c \cdot \delta\varepsilon_c, \tag{2.9}$$

because of the convexity of the yield function, which implies that $F_l \leq F_c$. Therefore F_l is a lower bound on the actual collapse load, F_c.

2.1.3 Proof of Upper Bound Theorem

The proof of the upper bound theorem is very similar to that of the lower bound theorem. Figure 2.2 shows a hypothetical failure criterion for a perfectly plastic soil. The subscript c again indicates the actual stresses and strains during collapse, while the subscript u indicates the stresses and strains corresponding to the upper bound estimates. The figure shows that both σ_c and σ_u vectors are touching the failure surface because either stress would cause collapse. The reader will note that here, as opposed to the lower bound proof, the component of incremental strain, $\delta\varepsilon$, can be drawn from the head of the σ_u vector, since it also causes collapse; therefore $\delta\varepsilon_u$ is drawn normal to the failure surface at this point in accordance with the associated flow rule.

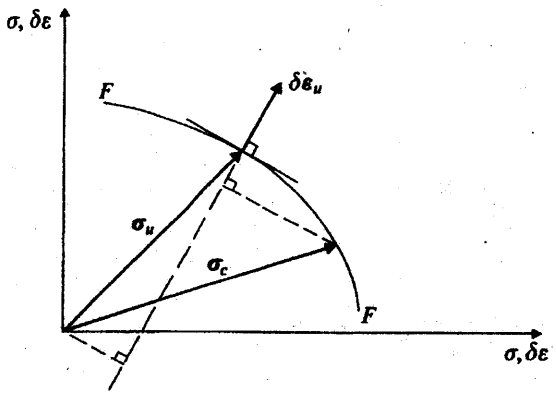

Figure 2.2 Proof of the Upper Bound Theorem (Atkinson and Bransby, 1978).

The principle of the upper bound theorem says that collapse must have occurred if

$$\sum F_u \cdot \delta w_u = \int_V \sigma_u \cdot \delta \varepsilon_u dV, \tag{2.10}$$

which has the same form as the equation of virtual work. Therefore, we can also write

$$\sum F_c \cdot \delta w_u = \int_V \sigma_c \cdot \delta \varepsilon_u dV \tag{2.11}$$

from the principle of virtual work and compare this to equation 2.10.

Again assuming that $\delta\varepsilon_u$ has a value of unity, the dot products on the right hand side of equations 2.10 and 2.11 become the components of the corresponding stress vectors, σ_u and σ_c, in the direction of the incremental strain, $\delta\varepsilon_u$, as shown by the constructions in the figure. These constructions reveal that that

$$\sigma_u \cdot \delta \varepsilon_u \geq \sigma_c \cdot \delta \varepsilon_u \tag{2.12}$$

because of the convexity of the yield function, which implies that $F_u \geq F_c$. Therefore F_u is an upper bound on the actual collapse load, F_c.

2.1.4 Treatment of Non Perfectly Plastic Materials

The proofs just discussed assume Equation 2.5 is valid for the relevant material. Actually, for this assumption to hold for a Mohr-Coulomb shear strength criterion, the angle of dilation, ψ, must equal to the soil's friction angle, ϕ. This requirement does not present a problem in undrained loading (for undrained stability of clay $\psi = 0$ and $\phi = 0$). However, the requirement does present a problem when loading is drained, since generally $\psi \neq \phi$. Consequently, equation 2.5 no longer holds because the failure criterion

is no longer a plastic potential, and the integrity of the limit theorems is compromised. For this reason, it is necessary to address this issue before proceeding to use limit theorems with confidence in a soil mechanics context.

For upper bound theorem, this problem is easily avoided because there is a theorem in plasticity that says:

> "Any set of loads which causes collapse for a perfectly plastic material for which the normality condition holds [$\psi = \phi$] will also cause collapse for a material with the same failure criterion, but for which vectors of strain increment at failure are not normal to the failure envelope."
> (Atkinson, 1978)

This is implicitly considered in the proof of the upper bound theorem discussed above, since the proof did not require anything to be said about the actual incremental strain at failure, $\delta\varepsilon_c$, even though the normality condition was still assumed when drawing $\delta\varepsilon_u$.

The same logic cannot be applied to the lower bound proof because the proof depends on the normality of $\delta\varepsilon_c$ to the failure criterion. An assumption is needed to avoid the problem that arises for drained loading. Therefore, we assume that

$$\psi = \phi, \tag{2.13}$$

so that equation 2.5 still holds and the proof of the lower bound theorem is still valid. A major disadvantage of this assumption is that the calculated lower bound of the problem is theoretically no longer a rigorous lower bound. However, Palmer (1966) suggested that this assumption gives an accurate lower bound for a soil with the same friction angle, ϕ, but with $\psi = 0$. We can now apply limit theorems to soils.

2.2 Numerical Limit Analysis

The author has used computer programs to solve limit theorems for an excavation problem based on the formulations proposed by Sloan (1988) and Sloan and Kleeman (1995). The original formulations have been modified by Ukritchon (1998) to account for the strength of structural members involved in the problem, such as footings or walls. This section sets up the optimization problem corresponding to each of the limit theorems when applied only to soil.

2.2.1 Numerical Formulation of the Lower Bound Method

The lower bound estimate requires a statically admissible stress field. To guarantee a statically admissible stress field, it is necessary to impose the restrictions that characterize static admissibility, i.e. equilibrium conditions, boundary conditions, and conditions imposed by failure criteria. These conditions appear in this formulation as constraints on the nodal stresses. These constraints are discussed in the following sections.

Since any statically admissible stress field produces a lower bound estimate, then the best lower bound estimate is one that maximizes the external loads of a statically admissible stress field. The formulation of this optimization problem for the lower bound theorem in plain strain is covered in this section, and is taken from Ukritchon (1996), Ukritchon (1998), and Sloan (1995).

2.2.1.1 Discretization

First, the soil is discretized into triangular elements defined by three nodes[2] as shown in Figure 2.3. Unlike other finite element discretization schemes, here each node is unique to a triangular element.

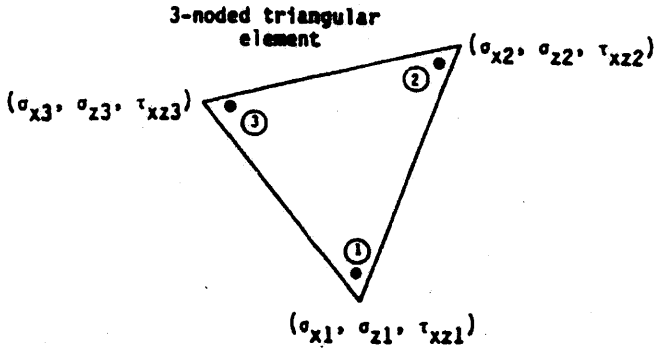

Figure 2.3 Typical Lower Bound Triangular Element (Sloan and Kleeman, 1995)

[2] The lower bound formulation generally also uses what are known as extension elements to simulate a soil continuum. These elements may have four nodes. However, extension elements were not used in this project and are not discussed here. The reader is referred to Ukritchon (1996) for further information on extension elements.

Each node has a σ_x, σ_y, and τ_{xy} associated with it as shown in Figure 2.3 (denoted σ_{xi}, σ_{yi}, and τ_{xyi}). Stresses are allowed to vary linearly within each element such that the stresses at any point in the element are given by:

$$\begin{aligned}\sigma_x &= \sum_{i=1}^{3} N_i \sigma_{xi} \\ \sigma_y &= \sum_{i=1}^{3} N_i \sigma_{yi} \\ \tau_{xy} &= \sum_{i=1}^{3} N_i \tau_{xyi},\end{aligned} \tag{2.14}$$

where N_i are standard linear shape functions given by:

$$\begin{aligned}N_1 &= \frac{(x_2 y_3 - x_3 y_2) + (y_{23} x + x_{32} y)}{2\left|(x_1 - x_3)(y_2 - y_3) - (x_3 - x_2)(y_3 - y_1)\right|} \\ N_2 &= \frac{(x_3 y_1 - x_1 y_3) + (y_{31} x + x_{13} y)}{2\left|(x_1 - x_3)(y_2 - y_3) - (x_3 - x_2)(y_3 - y_1)\right|} \\ N_3 &= \frac{(x_1 y_2 - x_2 y_1) + (y_{12} x + x_{21} y)}{2\left|(x_1 - x_3)(y_2 - y_3) - (x_3 - x_2)(y_3 - y_1)\right|},\end{aligned} \tag{2.15}$$

and

$$\begin{aligned}x_{32} &= x_3 - x_2 \\ x_{13} &= x_1 - x_3 \\ x_{21} &= x_2 - x_1 \\ y_{23} &= y_2 - y_3 \\ y_{31} &= y_3 - y_1 \\ y_{12} &= y_1 - y_2.\end{aligned} \tag{2.16}$$

Figure 2.4 shows an example of a final discretized section.

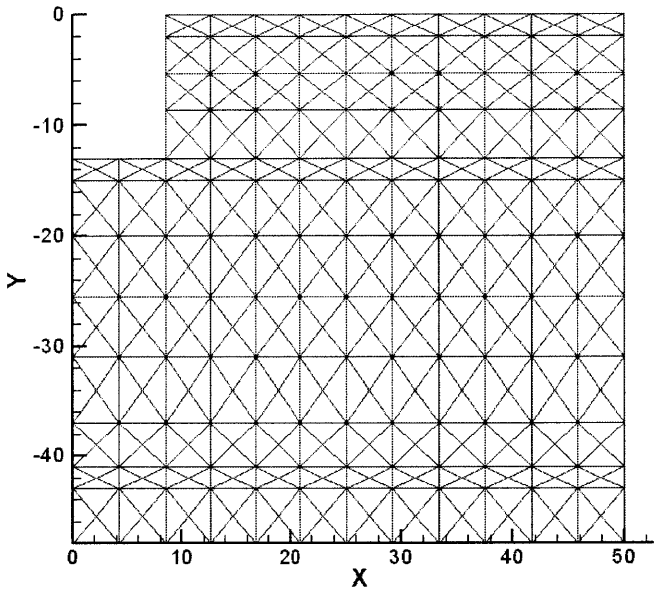

Figure 2.4 Example of a Discretized Section for an Excavation.

2.2.1.2 Equilibrium Conditions

The equations of equilibrium in two dimensions are given by:

$$\frac{\partial \sigma_{xx}}{\partial x} + \frac{\partial \tau_{xy}}{\partial y} = 0$$
$$\frac{\partial \tau_{yx}}{\partial x} + \frac{\partial \sigma_{yy}}{\partial y} = \gamma. \tag{2.17}$$

where γ is the gravitational body force. This constraint can be imposed on the nodal stresses by substituting the derivatives of Equation 2.14 into Equation 2.17. For three-noded elements, this results in two linear constraints that are conveniently represented in matrix form as

$$[A_1][\sigma_1] = [B_1], \tag{2.18}$$

where

$[A_1]$ is a matrix of linear coefficients resulting from the differentiation of equation 2.14,

$[\sigma_1]$ is the vector of the nodal stress components at the three nodes in an element in a Cartesian reference frame,

$[B_1]$ is the vector $[\, 0 \,,\, \gamma \,]^T$.

2.2.1.3 Stress Compatibility between Adjacent Elements

Static admissibility requires that the traction components of stress at a point be unique on a given plane; therefore, tractions along the interfaces between adjacent elements must be equal. The author refers to this as stress compatibility.

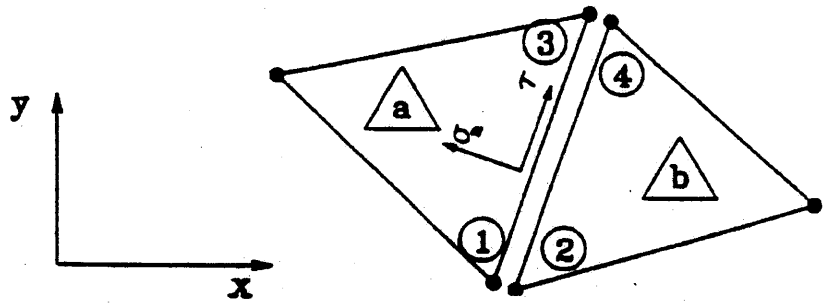

Figure 2.5 Stresses at Interfaces between Adjacent Elements (Sloan and Kleeman, 1995)

Figure 2.5 shows the interface of two adjacent elements. Because stresses vary linearly within each element, it is only necessary that the tractions at the two points defining the interface be equal. For example, for the elements in Figure 2.5,

$$\begin{aligned} \sigma_{n1} &= \sigma_{n2} \\ \sigma_{n3} &= \sigma_{n4} \\ \tau_1 &= \tau_2 \\ \tau_3 &= \tau_4. \end{aligned} \tag{2.19}$$

Or, more generally, this constraint can be written as

$$\begin{aligned} \sigma_{ni} &= \sigma_{nj} \\ \tau_i &= \tau_j, \end{aligned} \tag{2.20}$$

where i and j represent a pair of nodes on one end of an interface of adjacent elements.

This condition guarantees that the tractions are compatible along the length of the interface. To write the constraint on the nodal stresses for this condition, it is necessary to transform these tractions into their Cartesian components by using the standard transformation equations:

$$\begin{aligned} \sigma_n &= \sin^2\theta\sigma_x + \cos^2\theta\sigma_y - \sin 2\theta\tau_{xy} \\ \tau &= -\sin\theta\cos\theta\sigma_x + \sin\theta\cos\theta\sigma_y + \cos 2\theta\tau_{xy}, \end{aligned} \tag{2.21}$$

where θ describes the orientation of the interface. The constraint can then be written in matrix form as

$$[A_2][\sigma_2]=[B_2], \tag{2.22}$$

where

$[A_2]$ is a matrix of linear coefficients resulting from equation 2.21,[3]
$[\sigma_2]$ is the vector the nodal stress components at the four nodes defining an interface in a Cartesian reference frame,
and $[B_2]$ is the vector $[\,0\,,0\,,0\,,0\,]^T$.

The reader should note that this condition only imposes constraints on the *tractions* along interfaces; it does not impose constraints on any other component of the stress tensor. This gives rise to an interesting feature of the lower bound method: there will be stress discontinuities along the interfaces of adjacent elements.

2.2.1.4 Stress Boundary Conditions

Static admissibility also requires that stress boundary conditions be satisfied along boundaries where they are prescribed. Stress boundary conditions can be either uniform (constant) or linear.

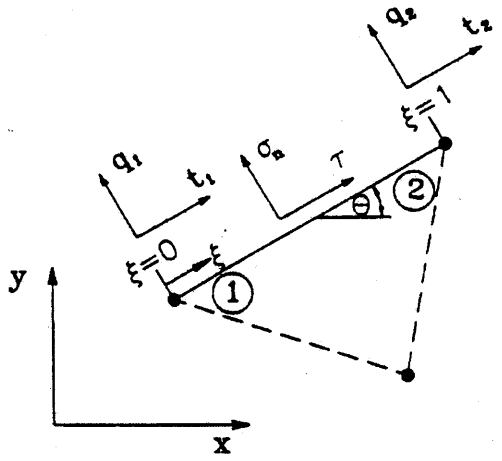

Figure 2.6 Stress Boundary Conditions (Sloan and Kleeman, 1995)

Figure 2.6 shows an example of a stress boundary condition. Stress boundary conditions are handled in the same way as stresses at interfaces of adjacent elements (Section 2.2.1.3). That is, the tractions on a boundary edge must be equal to the tractions imposed by boundary conditions at both ends of the boundary edge. Again, this

[3] The matrix $[A_2]$ is constructed such that the *difference* of the tractions of a nodal pair defining an end of the interface is calculated. Because the tractions in a nodal pair should be equal, this difference is zero, which is why $[B_2]$ is a zero vector.

guarantees that the boundary condition is satisfied along the length of the boundary edge because stresses vary linearly through the elements. Therefore, boundary conditions can be specified as:

$$\begin{aligned} \sigma_{ni} &= q_i \\ \sigma_{nk} &= q_k \\ \tau_i &= t_i \\ \tau_k &= t_k, \end{aligned} \tag{2.23}$$

where

q and t are the normal and shear components of the surface traction vector,
and i and k are nodes at either end of a boundary edge,

The reader should note the similarity between equation 2.23 and equation 2.20.

These nodal tractions are then transformed into their Cartesian components, and the constraint can again be conveniently expressed in matrix notation as

$$[A_3][\sigma_3] = [B_3], \tag{2.24}$$

where

$[A_3]$ is a matrix of linear coefficients again resulting from equation 2.23,[4]
$[\sigma_3]$ is the vector the nodal stress components at the two nodes defining a boundary edge in a Cartesian reference frame,
and $[B_3]$ is the vector $[q_i, t_i, q_j, t_j]^T$.

2.2.1.5 Failure Criteria

Finally, static admissibility requires that the stresses not exceed the failure criteria anywhere in the soil mass. For this project, the soil has a Mohr-Coulomb failure criterion:

$$\tau = c' + \sigma' \tan \phi'. \tag{2.25}$$

Equation 2.25 can be rewritten in a more convenient form by defining a function, F, as follows:

[4] The matrix $[A_3]$ cannot be constructed as a difference of tractions like $[A_2]$ because the boundary conditions are prescribed as constants (equation.2.25) instead of linear functions. This explains why $[B_3]$ is the vector of the tractions on the boundary edge and not a zero vector like $[B_2]$.

$$F = \left| \frac{\sigma_1 - \sigma_3}{2} - \left(\frac{\sigma_1 + \sigma_3}{2} \right) \sin\phi \right| - c\cos\phi. \tag{2.26}$$

It is not difficult to show F has the following properties:

1. When $F = 0$, failure occurs.
2. When $F < 0$, failure does not occur.
3. $F > 0$ is unattainable.

Equation 2.28 can then be rewritten in terms of the Cartesian stresses by standard transformations as follows:

$$F = (\sigma_y - \sigma_x)^2 + (2\tau_{xy})^2 - \left[2c\cos\phi + (\sigma_x + \sigma_y)\sin\phi \right]^2. \tag{2.27}$$

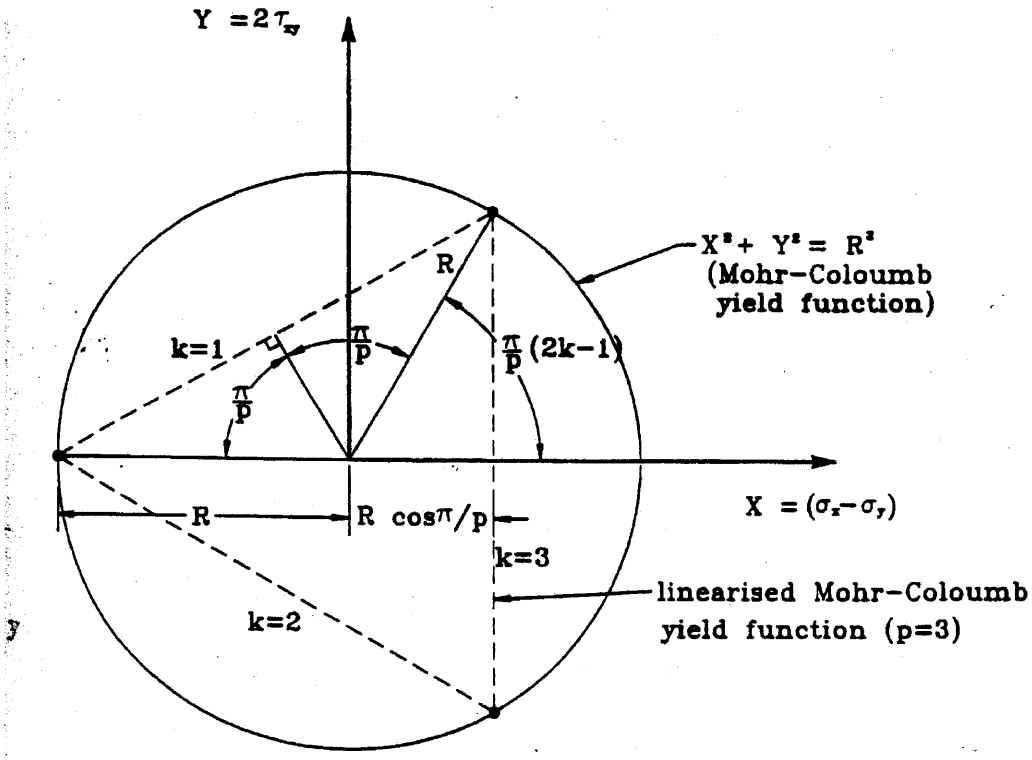

Figure 2.7 Linearization of Failure Criterion for Lower Bound (Sloan and Kleeman, 1995)

Equation 2.27 describes a non-linear relation among the stress components. The current formulation is based on a linear programming framework, so the yield function must be linearlized. To do this, stresses are conveniently transformed as follows:

$$
\begin{aligned}
X &= \sigma_y - \sigma_x \\
Y &= 2\tau_{xy} \\
R &= 2c\cos\phi + (\sigma_x + \sigma_y)\sin\phi,
\end{aligned}
\tag{2.28}
$$

such that the yield criterion can be represented as a circle in (X,Y) space:

$$X^2 + Y^2 = R^2. \tag{2.29}$$

To linearize this failure criterion, an equidimensional polygon is inscribed into this circle. The polygon is inscribed on the inside of the circle, as shown in Figure 2.7, to guarantee rigorous lower bound solutions. The new linearized failure criterion can be written as:

$$F_k \le A_k\sigma_x + B_k\sigma_y + C_k\tau_{xy} - D, \tag{2.30}$$

where

$$
\begin{aligned}
&p = \text{number of sides of the polygon} \\
&k = 1...p \\
&A_k = \cos(2\pi k / p) + \sin\phi\cos(\pi / p) \\
&B_k = \sin\phi\cos(\pi / p) - \cos(2\pi k / p) \\
&C_k = 2\sin(2\pi k / p) \\
&D = 2c\cos\phi\cos(\pi / p).
\end{aligned}
\tag{2.31}
$$

Since the friction angle is constant (and cohesion can vary linearly through the elements), all the terms in the right side of equation 2.30 vary linearly, so F also varies linearly. Therefore, to guarantee that the yield condition is not exceeded anywhere in an element, it is only necessary to impose the constraints specified by 2.30 on the nodal stresses. Since k varies from 1 to p, Equation 2.30 imposes p linear yield constraints for each node in the mesh. Since these constraints are linear, they can also be written simply in matrix form as

$$[A_4][\sigma_4] = [B_4], \tag{2.32}$$

where

$[A_4]$ is a matrix of the linear coefficients of equation 2.30,
$[\sigma_4]$ is the vector of the nodal stress components at the three nodes in an element in a Cartesian reference frame,
and $[B_4]$ is the vector $[\, D_i\,, D_i\,, \ldots\,, D_i\,]^T$.

2.2.1.6 Objective Function

Optimization of the lower bound load is achieved by maximizing the external loads in a statically admissible stress field. The external loads are determined by integrating the normal nodal stresses along the boundary of interest as follows:

$$Q_{ext} = \int_s \sigma_n ds. \tag{2.33}$$

Because stresses vary linearly, we can write Equation 2.33 as

$$Q_{ext} = \frac{L}{2}(\sigma_i + \sigma_k), \tag{2.34}$$

where i and k are the two nodes defining the edge of interest. In order to get σ_i and σ_k from their respective Cartesian components, we must again use the transformation equations, and Equation 2.34 can then be written in matrix form as

$$Q_{ext} = [c][\sigma_5] \tag{2.35}$$

where

- $[c]$ is the matrix of linear coefficients resulting from the transformation equations
- $[\sigma_5]$ is the vector of the nodal stress components at the two nodes defining the edge in a Cartesian reference frame,

For the purpose of excavations, which are the focus of this paper, the external load of interest is the vertical stress caused by the retained soil at the excavated grade elevation:

$$\sigma_v = \sum_{i=1}^{n} \gamma_i H_i \tag{2.36}$$

where γ_i and H_i are the unit weights and layer thickness corresponding to each layer respectively.

At this point, we note that there is a single representative unit weight, $\bar{\gamma}_l$, that will result in a vertical stress equivalent to that of Equation 2.38, such that

$$\sigma_v = \bar{\gamma}_l \sum_{i=1}^{n} H_i. \tag{2.37}$$

Since B_i are given, $\bar{\gamma}_l$ is the only variable in Equation 2.39. Therefore, for excavations, the objective function seeks to maximize $\bar{\gamma}_l$.

Because the vertical stress at the excavation depth occurs along a horizontal line, there is no need for transformations because σ_v is simply σ_y at any of the nodes at the depth of the excavation. Consequently, the objective function for excavations can be rewritten as

$$Q_{ext} = [c]\left[\bar{\gamma}_l\right], \tag{2.38}$$

where $[c]$ is the vector [1]. Equation 2.38 is maximized to obtain the best lower bound estimate.

2.2.1.7 Assembly of Complete Optimization Problem

As we have mentioned, the objective here is to maximize the external loads given the constraints of static admissibility. The complete problem formulation can then be written as:

Maximize:
$[c]\left[\bar{\gamma}_l\right]$
Subject to:
$[A_1][\sigma_1] = [B_1]$
$[A_2][\sigma_2] = [B_2]$
$[A_3][\sigma_3] = [B_3]$
$[A_4][\sigma_4] = [B_4]$

Table 2.1 Summary of Lower Bound Optimization Problem

2.2.2 Numerical Formulation of the Upper Bound Method

The upper bound estimate requires a kinematically admissible velocity (or displacement) field. This can be achieved by imposing velocity boundary conditions and restrictions on the flow rule. These conditions appear in this formulation as constraints on the nodal velocities, which are discussed in the following sections.

Since any kinematically admissible velocity field produces an upper bound estimate, then the best upper bound estimate is one that minimizes the external loads in a kinematically admissible velocity field. The formulation of this optimization problem in plain strain is covered in this section, and is taken mostly from Ukritchon (1998) and Sloan (1995).

2.2.2.1 Discretization

In this paper, the meshes that were utilized for the upper bound analysis were identical to those of the lower bound analysis. That is, the nodal coordinates of the upper bound mesh for a particular case are identical to those of the lower bound mesh.[5] However, the variables associated with each node are different.

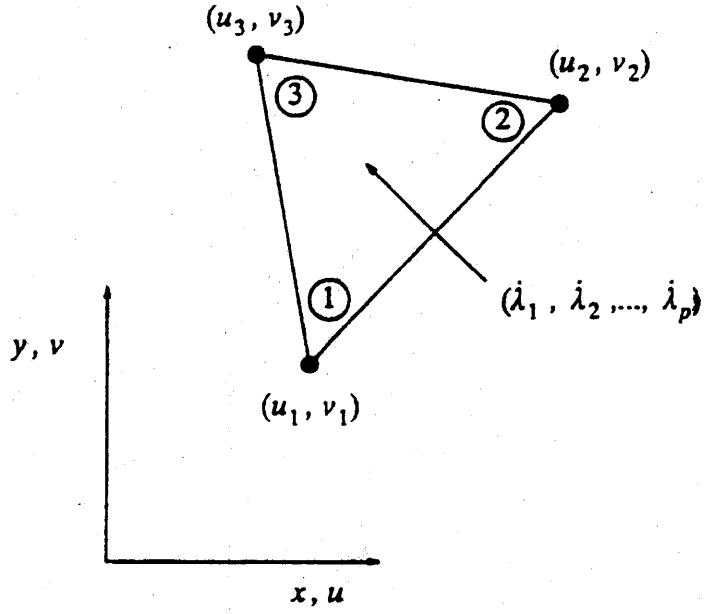

Figure 2.8 Typical Element in an Upper Bound Mesh (Sloan and Kleeman, 1995)

Figure 2.8 shows a typical element in an upper bound mesh. Each node has associated u and v components corresponding to velocities in the x and y direction respectively. These velocities are allowed to vary linearly within each element such that the velocities at any point in the element are given by:

[5] Lower bound analysis usually requires finer meshes for good lower bound estimates.

$$u = \sum_{i=1}^{3} N_i u_i$$
$$v = \sum_{i=1}^{3} N_i v_i, \tag{2.39}$$

where

(u_i, v_i) are the nodal point velocities,
and N_i are standard linear shape functions that were given in 2.15.

2.2.2.2 Flow Rule Constraints Within 3-Noded Elements

Section 2.1 showed that the associated flow rule is an inherent assumption of the upper and lower bound theorems. The flow rule is not explicitly observed in the lower bound formulation because the lower bound theorem deals only with the conditions of static admissibility. In the upper bound theorem, on the other hand, the flow rule imposes the first set of constraints on nodal velocities.

The components of *engineering* strain rates in Cartesian coordinates (with positive in compression sign convention) are given by:

$$\dot{\varepsilon}_x = -\frac{\partial u}{\partial x}$$
$$\dot{\varepsilon}_y = -\frac{\partial v}{\partial y} \tag{2.40}$$
$$\dot{\gamma}_{xy} = -\left(\frac{\partial u}{\partial y} + \frac{\partial v}{\partial x}\right).$$

Incremental strains (i.e. linearized strain rates) are given by the flow rule:

$$\Delta\dot{\varepsilon}_x = \Delta\dot{\lambda}\frac{\partial F}{\partial \sigma_x}$$
$$\Delta\dot{\varepsilon}_y = \Delta\dot{\lambda}\frac{\partial F}{\partial \sigma_y} \tag{2.41}$$
$$\Delta\dot{\gamma}_{xy} = \Delta\dot{\lambda}\frac{\partial F}{\partial \tau_{xy}},$$

where λ is the scalar plastic multiplier and F is the yield function defined by Equation 2.27.

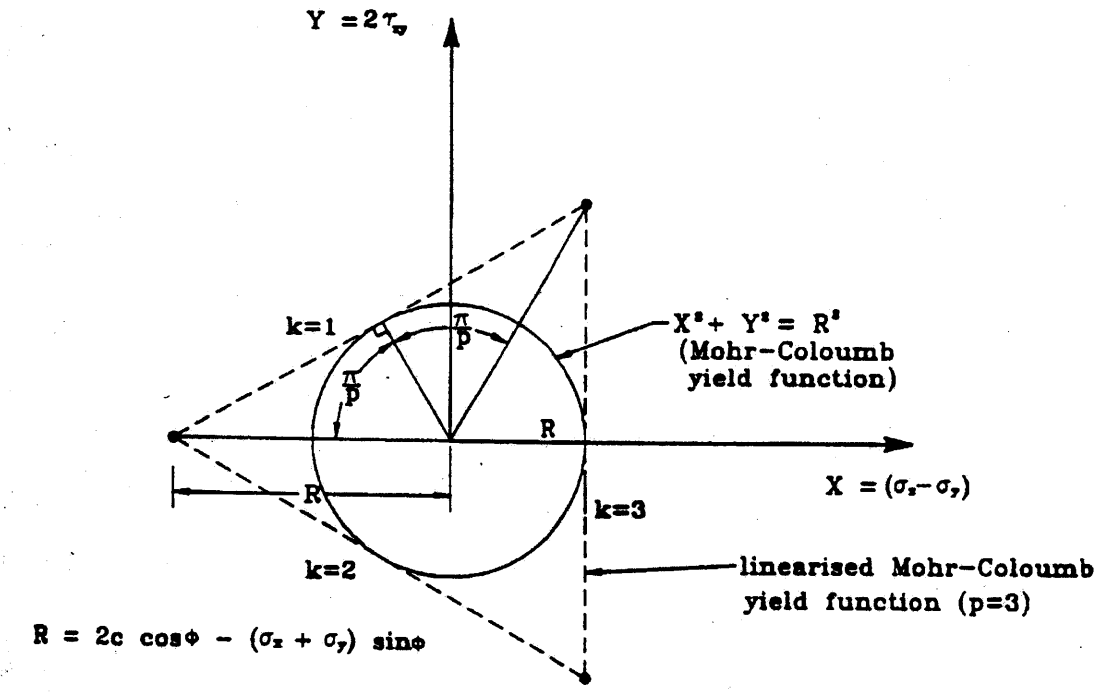

Figure 2.9 Linearization of Failure Criterion for Upper Bound (Sloan and Kleeman, 1995)

Combining Equations 2.40 and 2.41 gives velocity constraints. However, the yield criterion must first be linearized in order to use these equations within the linear programming framework. This is done using a polygonal linearization similar to lower bound formulation (Section 2.2.1.5) with one minor difference. Instead of inscribing the equidimensional polygon on the *inside* of the circular failure criteria, the polygon inscribed on the *outside*, as shown in Figure 2.9. This guarantees a rigorous upper bound estimate. Adjusting the procedure described in 2.2.1.5 to reflect this difference gives the following similar result:

$$F_k \le A_k \sigma_x + B_k \sigma_y + C_k \tau_{xy} - D, \tag{2.42}$$

where

$$
\begin{aligned}
&p = \text{number of sides of the polygon} \\
&k = 1 \ldots p \\
&A_k = \cos(2\pi k / p) + \sin\phi \\
&B_k = \sin\phi - \cos(2\pi k / p) \\
&C_k = 2\sin(2\pi k / p) \\
&D = 2c\cos\phi
\end{aligned}
\tag{2.43}
$$

Finally, differentiating Equations 2.39 and 2.42 and substituting the results into Equation 2.41 gives the following constraints on the nodal velocities:

$$
\begin{aligned}
&\sum_{i=1}^{3} \frac{\partial N_i}{\partial x} u_i + \sum_{k=1}^{p} \dot{\lambda}_k A_k = 0 \\
&\sum_{i=1}^{3} \frac{\partial N_i}{\partial y} v_i + \sum_{k=1}^{p} \dot{\lambda}_k B_k = 0 \\
&\sum_{i=1}^{3} \frac{\partial N_i}{\partial y} u_i + \sum_{i=1}^{3} \frac{\partial N_i}{\partial x} v_i + \sum_{k=1}^{p} \dot{\lambda}_k C_k = 0.
\end{aligned}
\tag{2.44}
$$

Equation 2.44 is usually reported in matrix form as

$$
[A_{11}][u_1] + [A_{12}]\left[\dot{\lambda}\right] = [0], \tag{2.45}
$$

where

$[A_{11}]$ is a matrix of the linear coefficients that result from differentiating the linear shape functions, N_i,

$[u_1]$ is the vector of the nodal velocity components at the three nodes in an element in a Cartesian reference frame,

$[A_{12}]$ is a matrix of the linear coefficients of equation 2.45,

$[\dot{\lambda}]$ is the vector $[\dot{\lambda}_1, \dot{\lambda}_2, \ldots, \dot{\lambda}_p]^T$,
and [0] is a zero vector $[0_1, 0_2, \ldots, 0_p]^T$.

2.2.2.3 Flow Rule Constraints At Element Interfaces

The upper bound approach essentially requires a failure mechanism for its calculation. Section 2.2.2.2 described the plastic flow constraints in zones of continuous straining (i.e., within an element). However, the formulation also allows velocity discontinuities in both normal and tangential strains (and velocities) along element interfaces. The velocity discontinuities must obey the flow rule.

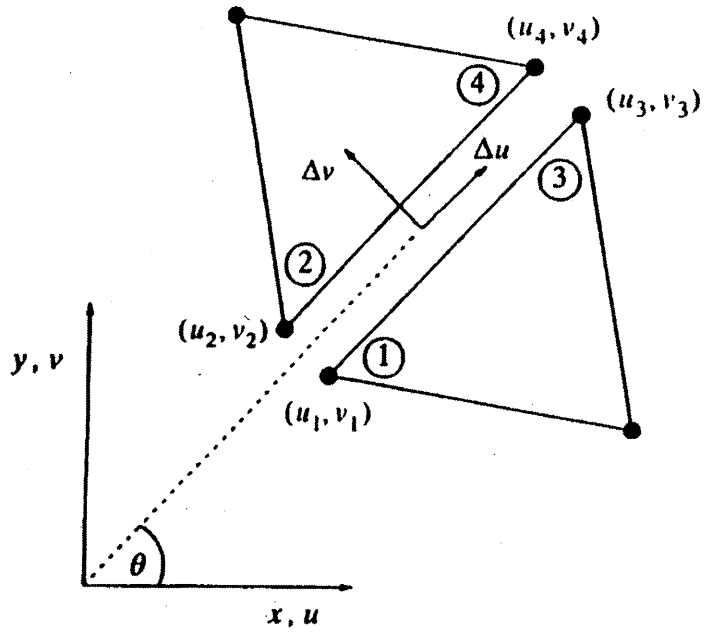

Figure 2.10 Velocities at Interfaces between Adjacent Elements (Sloan and Kleeman, 1995)

The flow rule at a velocity discontinuity for any Mohr-Coulomb material takes the form

$$\Delta v_n = |\Delta u_t| \tan\psi, \tag{2.46}$$

where Δv_n and Δu_t are the magnitudes of the normal and tangential velocity jumps respectively. As we mentioned in section 2.1.4, we assumed $\psi = \phi$, so Equation 2.46 becomes

$$\Delta v_n = |\Delta u_t| \tan\phi. \tag{2.47}$$

We can easily solve for Δv_n and Δu_t as functions of the nodal velocity components of a nodal pair to get

$$\begin{aligned} \Delta u_{ij,t} &= (u_j - u_i)\cos\theta + (v_j - v_i)\sin\theta \\ \Delta v_{ij,n} &= (u_i - u_j)\sin\theta + (v_j - v_i)\cos\theta \end{aligned} \tag{2.48}$$

where i and j represent a pair of nodes on one end of an interface of adjacent elements (e.g. nodes 1 and 2 in Figure 2.10), and θ is the inclination of the discontinuity measured from the horizontal.

At this point, a problem arises because the absolute value sign in equation 2.47 is not allowed within the linear programming framework. There are several ways to eliminate this problem, most of which require the direction of shearing along a discontinuity to be predetermined. This is clearly a disadvantage because the direction of shearing is usually not known beforehand, especially for large meshes. Sloan and Kleeman (1995) solved the problem by decomposing the tangential velocity jump into two auxiliary components:

$$\Delta u_t = u^+_t - u^-_t, \tag{2.49}$$

where u^+_t and u^-_t are both non-negative. Now consider the implications of the following definition:

$$|\Delta u_t| = u^+_t + u^-_t. \tag{2.50}$$

Clearly, 2.49 and 2.50 cannot be true simultaneously unless either u^+_t or u^-_t equals zero. We must consider when this will be the case.

Equation 2.50 can be rewritten as a piecewise function as follows:

$$\Delta u_t = \begin{cases} u^+_t + u^-_t & \text{if } \Delta u_t > 0 \\ u^+_t + u^-_t & \text{if } \Delta u_t = 0. \\ -u^+_t - u^-_t & \text{if } \Delta u_t < 0 \end{cases} \tag{2.51}$$

Setting equation 2.51 equal to 2.49 gives three systems of equations, each consisting of one equation and the two unknowns, u^+_t and u^-_t. These systems of equations will show that either one or both of the unknowns must be zero in all cases[6]; therefore we can apply definition 2.50 without introducing error.

Substituting the second equation of 2.48 and equation 2.50 into equation 2.47 gives the constraint

$$(u_i - u_j)\sin\theta + (v_j - v_i)\cos\theta = (u^+_{t,ij} + u^-_{t,ij})\tan\phi. \tag{2.52}$$

Equation 2.52 can now be written in matrix form as

$$[A_{21}][u_2] - [A_{22}]\left[u_\pm\right] = [0], \tag{2.53}$$

where

[6] One of the unknowns always cancels out.

$[A_{21}]$ is a matrix of the linear coefficients that result from the left side of equation 2.52,

$[u_2]$ is the vector of the nodal velocity components at the four nodes defining an interface in a Cartesian reference frame,

$[A_{22}]$ is a matrix of the linear coefficients that result from the right side of equation 2.52,

$[u_{\pm}]$ is the vector $[\ u^{+}_{t,ij}\ ,\ u^{-}_{t,ij}\ ,\ u^{+}_{t,kl}\ ,\ u^{-}_{t,kl}\ ]^{T}$,

$[0]$ is a zero vector,

and i, j and k, l represent the pairs of nodes at either end of an interface of adjacent elements (e.g. 1,2 and 2,4 in Figure 2.10)

2.2.2.4 Velocity Boundary Conditions

Prescribed velocity boundary conditions must also be satisfied to achieve kinematic admissibility. If a boundary condition is specified on an edge, it is only necessary that these conditions be satisfied on the nodes defining that edge, since velocities vary linearly through elements. Therefore, prescribed velocity boundary conditions will impose a nodal constraint in the form

$$\begin{aligned} u_i &= \bar{u} \\ v_i &= \bar{v} \end{aligned} \tag{2.54}$$

This constraint can also be written in matrix form as

$$[A_3][u_3] = [B_3], \tag{2.55}$$

where

$[A_3]$ is the identity matrix (since Equation 2.54 is in Cartesian coordinates),

$[u_3]$ is the vector of nodal velocity components at the boundary node in a Cartesian reference frame,

and $[B_3]$ is a zero vector $[\ \bar{u}\ ,\ \bar{v}\ ]^{T}$,

2.2.2.5 Objective Function

To obtain an upper bound estimate, we must set the rate of internal energy dissipation equal to the rate of work done by external forces as follows:

$$W_i \le W_e$$
$$W_i = W_{ele} + W_{dis} \tag{2.56}$$
$$W_e = \int_L \sigma_n V_n dL + \int_V \gamma V dA$$

where

W_i is the rate of internal energy dissipation,
W_e is the rate of external work done,
W_{ele} is the rate of internal energy dissipation due to continuous straining within elements,
W_{dis} is the rate of internal energy dissipation due to slippage at velocity discontinuities,
σ_n is normal stress,
γ is the unit weight of the soil,
V_n and V are velocities in the directions of σ_n and γ respectively.

To obtain the best upper bound estimate, the external forces are minimized for a kinematically admissible velocity field. It is obvious from Equation 2.56 that we must minimize W_i (and hence W_e) to achieve this.

The internal rate of energy dissipation occurs both within elements and along velocity discontinuities. First consider the rate of energy dissipation within elements, which will be simply equal to the summation of the strain energy rates, or

$$W_{ele} = \int_A (\sigma_x \dot{\varepsilon}_x + \sigma_y \dot{\varepsilon}_y + \tau_{xy} \dot{\gamma}_{xy}) dA. \tag{2.57}$$

Alternately, linearized definitions of strain rates (Equation 2.44) can be used:

$$W_{ele} = \int_A \sum_{k=1}^{p} [\dot{\lambda}_k (A_k \sigma_x + B_k \sigma_y + C_k \tau_{xy})] dA. \tag{2.58}$$

At failure, $F=0$ and the term inside the parentheses of Equation 2.58 is equal to D (from Equations 2.42 and 2.42). Therefore 2.58 can be written in a condensed form:

$$W_{ele} = 2\cos\phi \sum_{k=1}^{p} \dot{\lambda}_k \int_A c dA. \tag{2.59}$$

As the cohesion, c, can vary linearly within each element, equation 2.59 can be written as

$$W_{ele} = 2\frac{A}{3}\cos\phi \sum_{k=1}^{p} \dot{\lambda}_k \sum_{i=1}^{3} c_i. \tag{2.60}$$

In matrix form, this becomes

$$W_{ele} = [c_2]\left[\dot{\lambda}\right], \tag{2.61}$$

where

$[c_2]$ is the vector of the cohesion values at the three element nodes multiplied by the linear coefficients of equation 2.60,

and $[\dot{\lambda}]$ is the vector $[\dot{\lambda}_1, \dot{\lambda}_2, \ldots, \dot{\lambda}_p]^T$.

Now let us consider the rate of energy dissipation at element interfaces. From the definition of work, we can write the general equation for the rate of energy dissipated at a velocity discontinuity:

$$W_{dis} = \int_L (|\tau \Delta u_t| + \sigma_n \Delta v_n) dL, \tag{2.62}$$

where Δu_t and Δv_n are given by Equation 2.48, and L is the length of the discontinuity. Now we can substitute Equation 2.47 into 2.62 and get

$$\begin{aligned} W_{dis} &= \int_L (|\tau \Delta u_t| - \sigma_n |\Delta u_t| \tan\phi) dL \\ &= \int_L \left[|\Delta u_t| (|\tau| - \sigma_n \tan\phi) \right] dL \\ &= \int_L \left[|\Delta u_t| (c + \sigma_n \tan\phi - \sigma_n \tan\phi) \right] dL \\ &= \int_L \left[|\Delta u_t| c \right] dL. \end{aligned} \tag{2.63}$$

The minus sign of the second σ_n in Equation 2.63 is due to the fact that σ_n and v_n act in opposite directions.

Now we can substitute Equation 2.50 into the result of Equation 2.63 to get

$$W_{dis} = \int_L c(u^+_t + u^-_t) dL. \tag{2.64}$$

To perform the integration, we must write the variables of the integrand as functions of their location along the discontinuity. Because c, u^+_t, and u^-_t are all linear terms, we can write

$$c = c_{ij} + \frac{x}{L}\left(c_{kl} - c_{ij}\right)$$

$$u^{+}_{t} = u^{+}_{ij} + \frac{x}{L}\left(u^{+}_{kl} - u^{+}_{ij}\right) \tag{2.65}$$

$$u^{-}_{t} = u^{-}_{ij} + \frac{x}{L}\left(u^{-}_{kl} - u^{-}_{ij}\right),$$

where

i, j and k, l represent the pairs of nodes at either end of an interface of adjacent elements (e.g. 1,2 and 2,4 in Figure 2.10),

and x is the distance along the discontinuity.

After substituting Equation 2.65 into 2.64, the integral becomes

$$W_{dis} = \int_0^L \left[c_{ij} + \frac{x}{L}\left(c_{kl} - c_{ij}\right)\right]\left[u^{+}_{ij} + \frac{x}{L}\left(u^{+}_{kl} - u^{+}_{ij}\right) + u^{-}_{ij} + \frac{x}{L}\left(u^{-}_{kl} - u^{-}_{ij}\right)\right] dx. \tag{2.66}$$

The results of this integration can again be expressed in matrix form to get

$$W_{dis} = [c_3][u_{\pm}] \tag{2.67}$$

where

$[c_3]$ is the matrix of linear coefficients resulting from the integration of Equation 2.66,

and $[u_{\pm}]$ is the vector $[\ u^{+}_{t,ij}\ ,\ u^{-}_{t,ij}\ ,\ u^{+}_{t,kl}\ ,\ u^{-}_{t,kl}\ ]$.

Finally, the total rate of internal energy dissipation can now be written as:

$$W_i = [c_2]\left[\dot{\lambda}\right] + [c_3][u_{\pm}] \tag{2.68}$$

The upper bound theorem says that this must also equal W_e. Therefore,

$$W_e = [c_2]\left[\dot{\lambda}\right] + [c_3][u_{\pm}] \tag{2.69}$$

As we have mentioned, we must minimize W_i (or consequently W_e) to obtain the best upper bound estimate. Therefore, Equation 2.69 gives the objective function of this minimization problem.

2.2.2.6 Optimization for Excavations

For the analysis of excavations, the external load of interest is the vertical stress caused by the retained soil at the depth of the excavation. More specifically,

$$\sigma_v = \int_0^H \gamma dy, \tag{2.70}$$

where H is the depth of the excavation.

At this point, we note that there is a single representative unit weight, $\bar{\gamma}_u$, that will result in a vertical stress equivalent to that of Equation 2.70, such that

$$\sigma_v = \bar{\gamma}_u \int_0^H dy. \tag{2.71}$$

Converting σ_v to a force per unit length, and then writing the corresponding equation for W_e and setting it equal to W_i gives:

$$W_e = -\bar{\gamma}_u \int_A V dA = W_i, \tag{2.72}$$

where

A is the cross-sectional area above the depth of the excavation,
and V is the velocity field in the direction of γ.

In order to solve for $\bar{\gamma}_u$, we enforce the following additional constraint on the velocities:

$$\int_A V dA = -1 \tag{2.73}$$

Finally, we can take advantage of the linear variation of velocities and write Equation 2.73 as

$$\sum_{e=1}^{r} \left(\frac{A_e}{3} \sum_{i=1}^{3} v_i \right) = -1, \tag{2.74}$$

where

e indicates all the elements above the depth of the excavation,
A_e is the area of the corresponding element
and v_i are the vertical velocities at the three nodes within e^{th} element.

In matrix form, Equation 2.74 can be written as

$$[A_4][u_4] = [B_4] \tag{2.75}$$

where

$[A_4]$ is a vector of the area of the elements above the excavation depth,
$[u_4]$ is the vector of the vertical velocities of the elements above the excavation depth,
and $[B_4]$ is the vector $[\,-1\,,\,-1\,,\,\ldots\,,\,-1\,]^T$

2.2.2.7 Assembly of Complete Optimization Problem

As we have mentioned, the objective here is to minimize the external loads given the constraints of kinematic admissibility. The complete problem formulation is given in the table below.

Maximize:
$[c_2]\left[\dot{\lambda}\right]+[c_3][u_\pm]$
Subject to:
$[A_{11}][u_1]+[A_{12}]\left[\dot{\lambda}\right]=[0]$
$[A_{21}][u_2]-[A_{22}]\left[u_\pm\right]=[0]$
$[A_3][u_3]=[B_3]$
$[A_4][u_4]=[B_4]$

Table 2.3 Summary of Upper Bound Optimization Problem

Chapter 3. Software Packages and Required Inputs

We have now set up the optimization problems in such a way that linear programming methods can be applied. Many researchers have focused on producing efficient ways to solve this large linear programming problem. As a result, two basic algorithms that have been developed that can handle these calculations: *i*) the revised simplex algorithm, and *ii*) the active set algorithm. Sloan (1988) discusses these two algorithms in detail, and suggests that the active set algorithm provides a particularly efficient means to solve this problem. The active set algorithm was originally developed by Best and Ritter (1985), and has since been modified by Sloan (1988), Ukritchon (1998), Prasad (2003), and others. The software that was used in this project uses an up-to-date version of the active set algorithm to solve the linear programming problem of numerical upper and lower bound limit analysis. For further details on the active set algorithm, the reader is referred to Sloan (1988).

This chapter discusses in detail the programs that were used to apply the limit theorems to the case study in Chapter 4. By doing so, this chapter provides the link that is often missing from publications on this subject between the theory and application of limit theorems using linear programming.

3.1 Programs for the Lower Bound Method

3.1.1 LBgen – Lower Bound Mesh Generator

LBgen is the name of the mesh generator for the lower bound optimization problem. The purpose of LBgen is basically to discretize the soil mass into three-noded triangular elements. Like all the analysis programs we discuss in this report, LBgen was written in FORTRAN 77. It can be executed from the DOS command line by the command **lbgen "FILENAME"** once in LBgen's directory, where FILENAME is the name of the corresponding input file.

To create a mesh, LBgen requires information about the geometry of the problem. Figure 3.1 is an abbreviated and annotated example of an input file required for LBgen (See Appendix A for full listing).[7]

```
23                  , total number of points defined
12                  , total number of regions defined by points
0                   , nsel (not required here)
0                   , transition zone (not required here)
3                   , number of boundary edges (where boundary conditions will be defined)
0                   , extension zone (not required here)
6                   , number of layers
4                   , number of beam segment that define the structural element
-------------------------------------------------------------------------------
1  0.0  -32         , node data, syntax: (node number / x coordinate / y coordinate)
2  0.0  -31
...
23 50   0.0
-------------------------------------------------------------------------------
1  1   1   7   4  2 , region data, syntax : (region number / region shape / Lower left node /...
2  1   6  16  15  2 , Upper right node  / Number of subdivisions in x direction /...
3  1   2   8   4  6 , Number of subdivisions in y direction)
...
12 1  13 23  15  2
-------------------------------------------------------------------------------
1  1   5             , boundary edge data, syntax: (boundary edge number / 1st node on boundary edge / ...
2  5  10             , 2nd node on boundary edge)
3 14  23
-------------------------------------------------------------------------------
1  0.0  -2           , layer data, syntax: (layer number / elevation of top of layer /
2  -2   -5.3         , elevation of bottom of layer)
...
6  -31  -37
-------------------------------------------------------------------------------
1  6   11            , beam segment data, syntax: (segment number / 1st node on beam segment / ...
2  11  12            , 2nd node on beam segment)
3  12  13
4  13  14
```

Figure 3.1 Abbreviated and Annotated LBgen Input File

The first eight lines of the input file provide summary information corresponding to the lower bound mesh. This information simply tells LBgen where to find a particular set of information (e.g. information about nodes) within this input file.[8]

The first data set LBgen requires is node coordinates. It is not necessary to define all the nodes in the mesh at this point. It is only necessary to define the nodes that define

[7] All the input files in the appendix were used in the MUNI case study in Chapter 4.

[8] LBgen is capable of generating extension and transition zones. Neither of these was needed in this project so they are not discussed here. LBgen can also generate meshes by using super elements (nsel). However, super elements are not required to create uniform meshes like the ones used in this project, so they are not discussed here.

regions of constant element size. The user should also keep in mind that layer changes, structural segments (referred to as beam segments), and strut locations are all ultimately defined by nodes, so nodes must be created wherever any of these are desired.

LBgen then requires information about the regions defined by the nodes. The region data consists of the geometry of each region (rectangular and triangular regions are discretized differently), the nodes defining each region, and the number of subdivisions desired for each region.[9]

Next, LBgen requires the user to define the boundary edges. These are not necessarily the outer edges defining the overall geometry of the problem; they are simply the edges in the mesh where the user wishes to prescribe a stress boundary condition. For excavations in plain strain, the centerline of the excavation corresponds to a line of symmetry with zero shear stress ($\tau = 0$). The stress-free ground surface (and excavated grade) must be specified with zero normal and shear stress ($\tau = 0, \sigma = 0$).

The user must then input the depths that define the extents of the soil layers. Material properties are not required at this point. Only the elevations defining the layers are necessary so that LBgen can associate each soil element with the material number of the corresponding layer.

Finally, LBgen requires information about location of beam segments in the section. Again, no material properties are needed at this point. It is only necessary to specify the nodes defining the beam segment so that LBgen can create nodes and joints to define its geometry.

The output of LBgen is a plain text file containing only information about the mesh. This output file must be modified so that it includes material properties, water tables, and stress boundary conditions. These modifications are discussed in the following section.

3.1.2 LBmain – Main Lower Bound Optimization Program

LBmain is the name of the program that solves the linear programming problem for the lower bound. The purpose of LBmain is basically to find the lower bound estimate and to produce results that can be plotted and analyzed. It can be executed from the DOS

[9] These subdivisions create the nodal coordinates for nodes not defined within this input file.

command line by the command **lbmain "FILENAME"** once in LBmain's directory, where FILENAME is the name of the corresponding input file.

The output file from LBgen is the input file for LBmain. This input file must first be augmented with material properties, water tables, and stress boundary conditions before it is used in LBmain.

Figure 3.2 is an abbreviated and annotated example of an input file required for LBmain (See Appendix B for full listing). The first line of the input file contains a set of commands that were taken as default for this project. The second and third lines provide summary information about the soil mass and beam elements respectively. This information simply tells LBmain where to find a particular set of information (e.g. material properties) within this input file.

This input file is set up in such a way that only its beginning (material properties and water tables) and end (stress boundary conditions) have to be modified as long as there is only one set of material properties for beam elements and all layers are horizontal. In this case, all beam elements are assigned the same material properties, and all elements within each layer are assigned their respective material properties. This default can be overridden manually by changing the set of material properties assigned to beam or soil elements in the corresponding section of the input file (refer to Appendix B).

Figure 3.2 shows the syntax that is used to input material properties, water tables, and stress boundary conditions. When the input file is complete, the user can run LBmain. LBmain gives a series of output files that can then be used to analyze and plot the results with plotting software, such as Tecplot. The text files also include $\bar{\gamma}_l$. The lower bound method only addresses stress equilibrium. Consequently, output data consist only of nodal stress data for the optimal statically admissible stress field.

```
1 F T T F
Print (int), mesh generation(T/F), Scale(T/F) , Steep(T/F), store (T/F)
4176 1 1392   0   0 2037  2  6  1
Soil Summary; Syntax: Number of: nodes, unique coordinates, triangular elements, triangular extension, rectangular extension, number of discontinuities, unit weights, material no, water tables
 40   20   18 3  1  , Beam Summary; Syntax: Number of : nodes, beam elements, joint element, support, material no
1 -1
2  1
Unit Weights; Syntax: Reference unit weight number, unit weight (negative unit weight indicates unit weight will be optimized)
1   ,Factor of safety
  1  1
   .000    0.0   0.0  30  1  24
...
  6  1
 -31.000 0.0  0.0  30  2  24.
Soil Material Properties;
Line 1; Syntax: Material reference number, soil type
Line 2; Syntax:
If soil type 1 (total stress analysis): reference elevation, S_u at reference elevation, gradient of S_u, friction angle, reference unit weight number, p (number of linear segments approximating failure criterion)
If soil type 3 (effective stress analysis): reference elevation, S_u at reference elevation, gradient of S_u, friction angle, reference unit weight number, reference water table, p (number of linear segments approximating failure criterion)
1  1
-2  9.81
Water Table Properties;
Line 1; Syntax: Reference water table number, water table type
Line 2; Syntax: if type 1 water table ( hydrostatic pore pressures): elevation of water tale, unit weight of water
1  1
882
Beam Material Properties;
Line 1; Syntax: Beam material reference number, beam material type
Line 2; Syntax: Type 1 (limited moment capacity only): moment capacity
Node coordinate information
Joint Information
Triangular element information
Discontinuity information
Beam element information
Joint information
       3        , number of boundary conditions
      24
  12   11   60   59  468  467  516  515  564  563  612  611
660  659  708  707 1836 1835 1884 1883
 1932 1931 2520 2519
CON  NONE
T
0.0  F
...
0.0  F
Boundary condition information for boundary edges
Line 1; Syntax: Number of nodes on boundary
Line 2; Syntax: List of nodes on boundary
Line 3; Type of boundary condition; Syntax: Type of shear boundary condition, type of normal boundary condition
Line 4; Syntax:
If NONE (no constraint along boundary): No information required
If CON (constant stress along boundary): Flag (T if value prescribed), Value of boundary stress, Flag (T if apply FS))
0 point loads (not used and not discussed)
0 int shear (not used and not discussed)
0 print out for nor,tau (not used and not discussed)
1
 3
 3467 3468 3469
 F T T
  0.0d0 F
  0.0d0 F
Support boundary conditions;
Line 1; Syntax: Number of joints
Line 2; Syntax: Joint Numbers
Line 3; Syntax: Flags shear, vertical, and moment support
Line 4; Syntax: Values of boundary condition, Flag (T if apply FS)
0 applied force at joint (not used and not discussed)
0 , distributed load for beams (not used and not discussed)
20 Number of soil-structure interfaces
3430
  108  107   41   42
F
...
F
Soil structure interaction;
Line 1; Syntax: Beam element number
Line 2; Syntax: Nodes defining interface
Line 3; Syntax: Flag for prescribed boundary condition on interface
Line 4; Syntax: Value of interface stress, Flag to apply factor of safety
```

Figure 3.2 Abbreviated and Annotated LBmain Input File

3.2 Programs for the Lower Bound Method

3.2.1 UBgen – Upper Bound Mesh Generator

UBgen is the name of the mesh generator for the upper bound optimization problem. The purpose of UBgen is basically to discretize the soil mass into three-noded triangular elements. The resulting mesh is slightly different than the one created by LBgen (principally because LBgen can create extension elements and transition zones) and boundary conditions are specified differently. UBgen can be executed from the DOS command line by the command **ubgen "FILENAME"** once in UBgen's directory, where FILENAME is the name of the corresponding input file.

To create a mesh, UBgen requires information about the geometry of the problem. Figure 3.3 is an abbreviated and annotated example of an input file required for UBgen (See Appendix C for full listing). The format for the UBgen input is almost identical to that of LBgen. The first seven lines of the input file provide summary information corresponding to the upper bound mesh. This information simply tells UBgen where to find a particular set of information within this input file.

Since neither transition zones nor extension zones were used in this project, the only difference between the format of the input files for UBgen and LBgen is the summary information at the beginning of the file. Otherwise, the format of the input files is identical. However, the user should keep in mind that boundary conditions are specified as velocities in the upper bound formulation; far field boundaries are defined by $u_i = v_i = 0$ and the centerline of the excavation is defined by $u_i = 0$.

```
23                  , total number of points defined
12                  , total number of regions defined by points
0                   , nsel (not required here)
3                   , number of boundary edges (where boundary conditions will be defined)
0                   , number of loads (not required here)
6                   , number of layers
4                   , number of beam segment that define the structural element
-------------------------------------------------------------------------------
1  0.0  -32         , node data, syntax: (node number / x coordinate / y coordinate)
2  0.0  -31
...
23 50   0.0
-------------------------------------------------------------------------------
1  1   1   7   4  2 , region data, syntax : (region number / region shape / Lower left node /...
2  1   6  16  15  2 , Upper right node / Number of subdivisions in x direction /...
3  1   2   8   4  6 , Number of subdivisions in y direction)
...
12 1  13 23  15  2
-------------------------------------------------------------------------------
1  5   1            , boundary edge data, syntax: (boundary edge number / 1st node on boundary edge / ...
2  1  15            , 2nd node on boundary edge)
3  15 23
-------------------------------------------------------------------------------
1  0.0  -2          , layer data, syntax: (layer number / elevation of top of layer /
2  -2   -5.3        , elevation of bottom of layer)
...
6  -31  -37
-------------------------------------------------------------------------------
1  6   11           , beam segment data, syntax: (segment number / 1st node on beam segment / ...
2  11  12           , 2nd node on beam segment)
3  12  13
4  13  14
```

Figure 3.3 Abbreviated and Annotated UBgen Input File

The output of UBgen is a plain text file containing only information about the mesh. This output file must be modified so that it includes material properties, water tables, and velocity boundary conditions. These modifications are discussed in the following section.

3.4 Ubmain - Main Upper Bound Optimization Program

UBmain is the name of the program that solves the linear programming problem for the upper bound. The purpose of UBmain is basically to find the upper bound estimate and to produce results that can be plotted and analyzed. It can be executed from the DOS command line by the command **ubmain "FILENAME"** once in UBmain's directory, where FILENAME is the name of the corresponding input file.

Figure 3.4 is an abbreviated and annotated example of an input file required for UBmain (See Appendix D for full listing). The first line of the input file contains a set of commands that were taken as default for this project. The second and third lines provide

summary information about the soil mass and beam elements respectively. This information simply tells UBmain where to find a particular set of information within this input file.

```
1 F T T F
Print (int), mesh generation(T/F), Scale(T/F) , Steep(T/F), store (T/F)
4176 1 1392 2069  2  6  1
Soil Summary; Syntax: Number of: nodes, unique coordinates, triangular elements, number of discontinuities, unit weights, material no, water tables
 40  20  21  1 , Beam Summary; Syntax: Number of : nodes, beam elements, joint element, material no
1 -1
2  1
Unit Weights; Syntax: Reference unit weight number, unit weight (negative unit weight indicates unit weight will be optimized)
1  ,Factor of safety
 1  1
  .000   0.0   0.0  30  1  24
...
 6  1
 -31.000 0.0  0.0  30  2  24.
Soil Material Properties;
Line 1; Syntax: Material reference number, soil type
Line 2; Syntax:
If soil type 1 (total stress analysis): reference elevation, S_u at reference elevation, gradient of S_u, friction angle, reference unit weight number, p (number of linear
segments approximating failure criterion)
If soil type 3 (effective stress analysis): reference elevation, S_u at reference elevation, gradient of S_u, friction angle, reference unit weight number, reference water
table, p (number of linear segments  approximating failure criterion)
1  1
-2  9.81
Water Table Properties;
Line 1; Syntax: Reference water table number, water table type
Line 2; Syntax: if type 1 water table ( hydrostatic pore pressures): elevation of water tale, unit weight of water
1  1
882
Beam Material Properties;
Line 1; Syntax: Beam material reference number, beam material type
Line 2; Syntax: if type 1 (limited moment capacity only): moment capacity
Node coordinate information
Joint Information
Triangular element information
Discontinuity information
Beam element information
Joint information
        3          , number of boundary conditions
24
 2519 2520 1931 1932 1883 1884 1835 1836 707  708  659  660  611  612  563  564  515  516  467  468   59   60   11   12
 T F
 .00 .00 .00 .00 .00 .00 .00 .00 .00 .00 .00 .00 .00 .00 .00 .00 .00 .00 .00 .00 .00 .00 .00 .00
...
 .00 .00 .00 .00 .00 .00 .00 .00 .00 .00 .00 .00 .00 .00 .00 .00 .00 .00 .00 .00 .00 .00 .00 .00 .00 .00 .00 .00 .00 .00 .00 .00 .00 .00 .00 .00 .00 .00
.00 .00
Boundary condition information for boundary edges
Line 1; Syntax: Number of nodes on boundary
Line 2; Syntax: List of nodes on boundary
Line 3; Type of boundary condition; Syntax: Flag  u, Flag for v (T if boundary condition present)
Line 4; Syntax: if flag = F, no information required; if flag = T, list of nodal velocity boundary conditions
0 distributed stress on boundary (not used and not discussed)
0 point loads (not used and not discussed)
1  ,vel bcs of joint
  3 ,#of joints
  3499 3500 3501
  T F F
  0.0
Support boundary conditions;
Line 1; Syntax: Number of joints
Line 2; Syntax: Joint Numbers
Line 3; Syntax: Flags u, v, and w
Line 4; Syntax: Values of boundary condition (if flag = T)
0 applied force at joint (not used and not discussed)
0 , applied stress for beams (not used and not discussed)
```

Figure 3.4 Abbreviated and Annotated UBmain Input File

This input file is also set up in such a way that only its beginning (material properties and water tables) and end (velocity boundary conditions) have to be modified as long as there is only one set of material properties for beam elements and all layers are

horizontal. In this case, all beam elements are assigned the same material properties, and all elements within each layer are assigned their respective material properties. This default be overridden manually by changing the set of material properties assigned to beam or soil elements in the corresponding section of the input file (refer to Appendix D).

Figure 3.4 shows the syntax that is used to input material properties, water tables, and velocity boundary conditions. Material properties and water tables use the same syntax used in the LBmain input files, while the syntax for boundary conditions changes slightly. When the input file is complete, the user can run UBmain. UBmain gives a series of output files that can then be used to analyze and plot the results with plotting software. The text files also include $\bar{\gamma}_u$. Output data consist only of the nodal point velocities for the optimal kinematically admissible stress fields.

3.5 Computation Times

The author did all of his analysis on a Pentium 4, 1.4GHz desktop computer. This section discusses the computation times required by the software based on the analysis of Chapter 4 and seven other cases the author briefly studied.

The mesh generators run practically instantaneously. For very coarse meshes, computation time can be as little as about 0.25 seconds. Even for very fine meshes like the ones used later in this paper, computation time never exceeded 3 seconds.

The computation time required for LBmain and UBmain to run is highly dependent on the coarseness of the mesh and the number of linear segments defining the failure criterion (p). For this project, the yield surface was always approximated by 24 linear segments (in order to achieve accurate representation of the yield criterion, Ukritchon 1996). However, the author experimented with a wide range of mesh coarseness in order to minimize the size of the range defined by $\bar{\gamma}_l$ and $\bar{\gamma}_u$. The author found that LBmain and UBmain generally require an equal amount of time to solve the linear programming problem for the same mesh. The time required for these programs to run ranged from about 1 second for a mesh containing 120 nodes to 63 minutes for a mesh containing 4176 nodes. More details concerning computation times are reported in Chapter 4.

Chapter 4. Stability of the Cut and Cover Excavation for the MUNI Metro Turnback (MMT) project

4.1 Background

The MUNI Metro Turnback project consisted of the construction of twin steel lined 5.48 m diameter tunnels extending 245 M South from the Embarcadero Station, marked AB in Figure 4.1. Section BC involved the construction of a cut and cover reinforced concrete box structure. The excavation required for this section is less than 30 M from the shore in some places and as little as 9 M away from settlement sensitive buildings (Koutsoftas et al., 2000). The excavation was 17 M wide and 11-13 M deep. The most critical sections with the deepest excavations were located close to the tunnel access shaft and were closely monitored during construction (marked 'Test Section' in Figure 4.1). This section shows the detailed analysis of the stability of the excavation at this location, and then compares the results of numerical limit analysis to those of limit equilibrium methods reported by Koutsoftas et al. (2000).

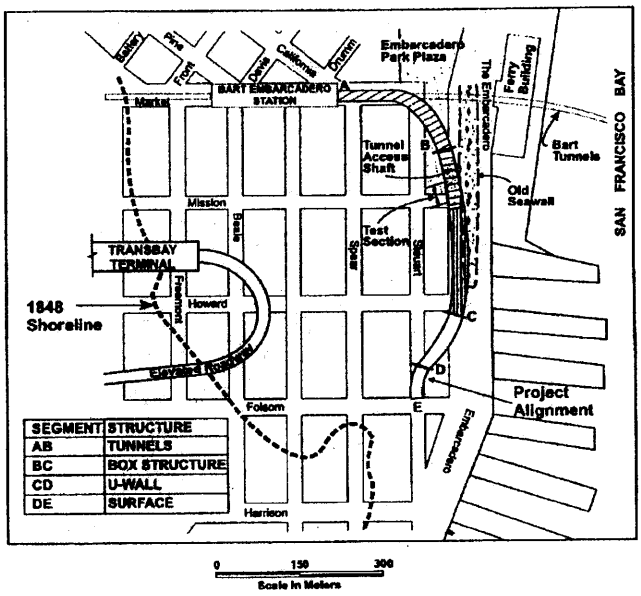

Figure 4.1 Map of MMT Site and Surrounding Area (Koutsoftas et al., 2000)

4.2 Soil Profile

Figure 4.2 shows a typical soil profile of the MMT site. The site has a level ground surface and is overlain by a 6 M thick layer of fill consisting of medium to fine

sand. The fill is very loose and contains variable amounts of debris. For analysis, this material was assumed to have zero cohesion and a friction angle of 30°. The groundwater table is typically about 2 M below the ground surface.

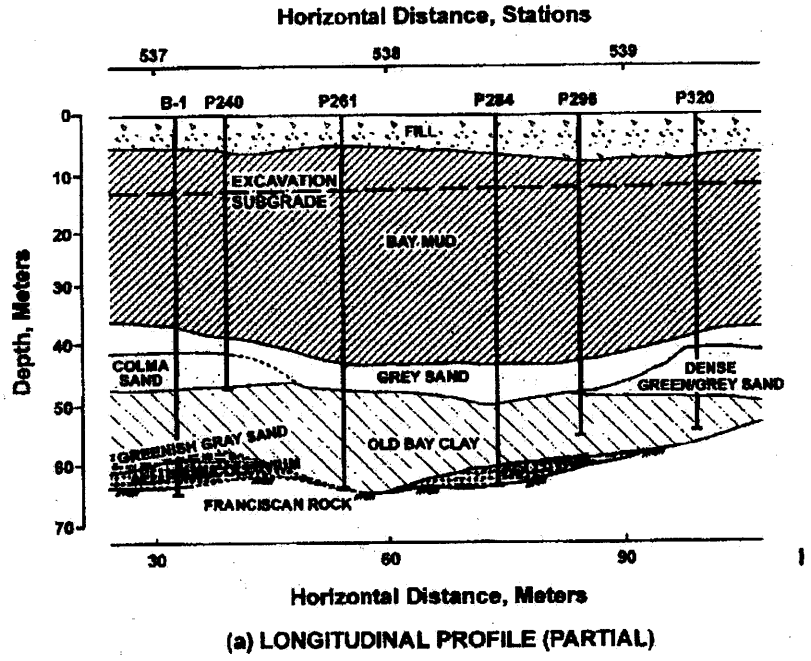

Figure 4.2 Typical Soil Profiles (Koutsoftas, 2000)

The fill is underlain by a 30-40 M thick layer of saturated clay locally known as Bay Mud. The Bay Mud is of primary importance as the base of the excavation extends only 7 M into the clay, and excavation stability depends on the properties of the underlying soil. Figure 4.3 summarizes the in situ stresses, stress history and undrained strength properties of the clay. The data show that the Bay Mud is normally consolidated above a depth of about 15 M, but becomes slightly overconsolidated below this depth. Koutsoftas et al. (2000) show that the undrained shear strength, Su, of the clay increases with depth in the Bay Mud, based on laboratory DSS and field vane tests. They assume these shear modes provide an average strength profile for the Bay Mud. The figure also shows estimated profiles for $S_{u,TC}$ and $S_{u,TE}$, the compression and extension shear strength profiles, assuming normalized soil properties (after Ladd and Foott, 1974). The current analysis is strictly based on the $S_{u,DSS}$ profile in Figure 4.3 and assumes isotropic shear strength of the clay. This is considered a reasonable approximation based on studies presented recently by Ukritchon et al. (2003).

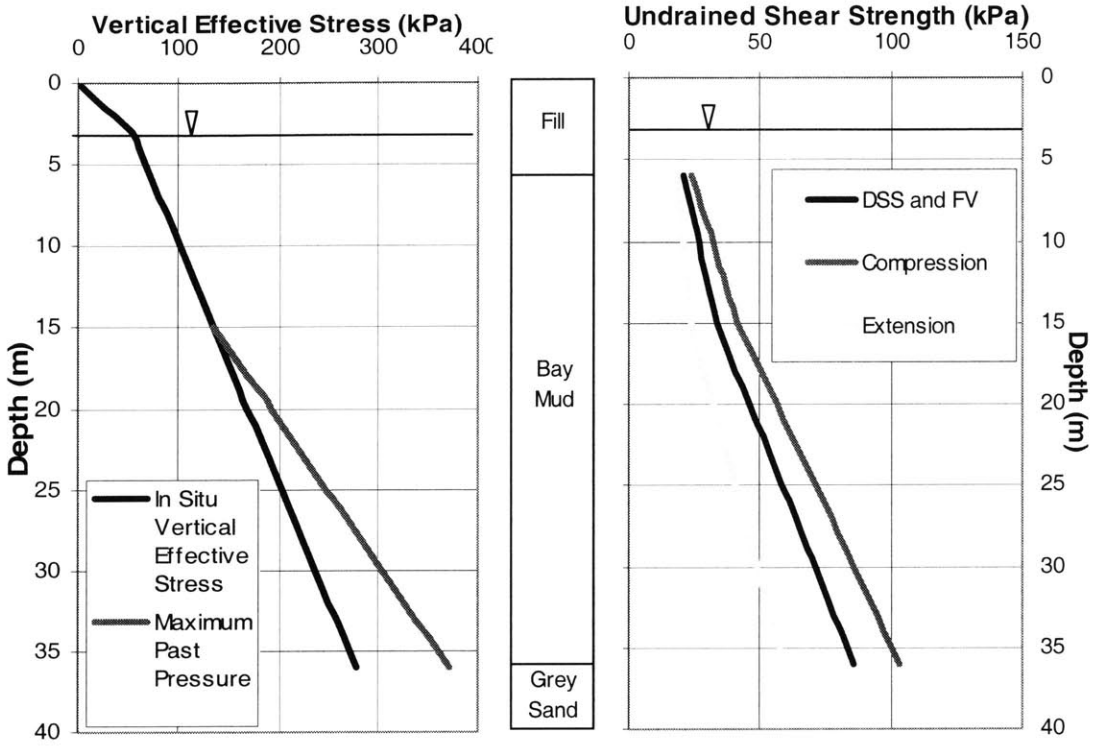

Figure 4.3 Strength Properties of Bay Mud (corrected from Koutsoftas et al., 2000)

The Bay Mud is underlain by a loose, fine marine sand known locally as Grey Sand. There are two lenses of denser sands underneath the Grey Sand. Both of these sands were present at the section of the excavation we will be analyzing. We assumed a friction angle of 30° for both sands.

These sands overly a stiff clay deposit known as Old Bay Clay that overlies the bedrock. Old Bay Clay has a uniform S_u = 85 kPa. The depth of the bedrock varies throughout the site from 35 to 60 M (Koutsoftas et al., 2000).

A section of the excavation and support system are shown on Figure 4.4. The figure shows the layers that were present at that section, the location of the struts, perimeter SPTC wall, and the depth of the excavation. Table 4.1 is a summary of the soil properties of the layers in the profile.

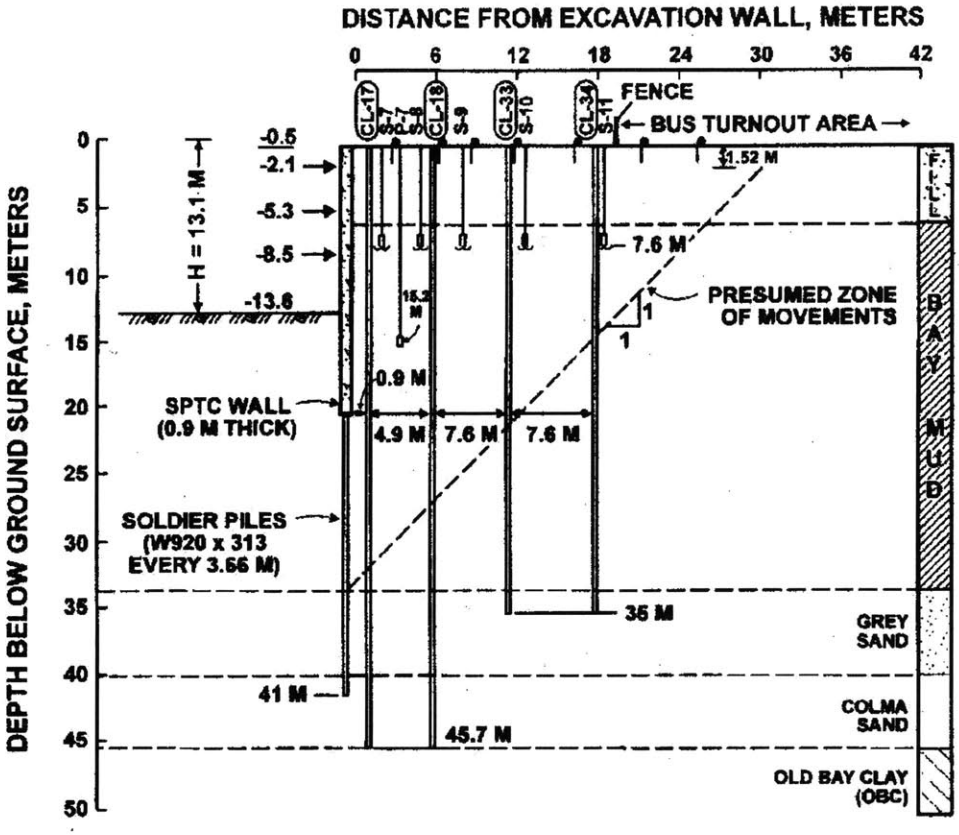

Figure 4.4 Excavation Section and Strut Locations (Koutsoftas et al., 2000)

Layer	Average S_u (kPa)	Φ (°)	Average γ (kN/m^3)
Fill	0	30*	18.3
Bay Mud	50	0	16.5
Grey Sand	0	30*	18
Colma Sand	0	30*	18
Dense Grey Sand	0	30*	18*
Old Bay Clay	85	0	18

***indicates soil properties that were assumed for analysis**

Table 4.1 Summary of Soil Properties of MMT Soil Profile

4.3 Excavation Support System

The excavation support system consisted of a Soldier Pile and Tremie Concrete (SPTC) wall with three levels of struts. Figure 4.5 is a diagram of the SPTC wall. The wall is 0.91 M thick and contains are W920 x 313 soldier piles sections placed at 3.66 M intervals. The concreted portion of the wall only extends to a depth of 20 M. Beyond that, the soldier piles alone extend to a depth of 41 M as shown in Figures 4.4 and 4.5.

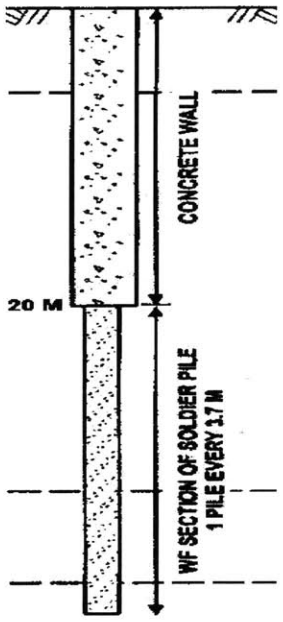

Figure 4.5 SPTC Wall Detail (Koutsoftas et al., 2000)

The strength of the wall, M_P = 0.88 MNm/m, was calculated based on the full plastic capacity of the soldier piles assuming a yield stress of σ_y = 414 MPa (60 ksi steel). The strength of the concrete was ignored in this calculation because the concrete is not sufficiently reinforced to span vertically and cannot carry moments in the vertical direction. The soldier piles are placed sufficiently close together so the wall has enough moment capacity in the horizontal direction to hold the retained soil and transfer the resulting horizontal forces to the soldier piles. The wall was supported by three levels of bracing as shown in Figure 4.4. The figure shows that the struts are placed at depths of 2.1, 5.3, and 8.5 M. Table 4.2 summarizes the relevant material properties of the SPTC wall.

M_p (MNm/m)	0.88

Table 4.2 Summary of Relevant Material Properties of SPTC Wall

4.4 Analysis Results and Comparison

4.4.1 Mesh Selection

In order to analyze the chosen section of the excavation, we first had to determine the adequate dimensional extents of the problem. Initially, the author considered a section of the excavation extending down to the Franciscan bedrock with lateral boundary located 100 M from the center of the excavation.

The sole purpose of this exercise was to help us focus the analysis on the area affected by instability. By doing this, the meshes can be refined specifically in this area and more precise bounds are obtained. Figure 4.6 shows the mesh that was used to evaluate this section along with the relevant boundary conditions.

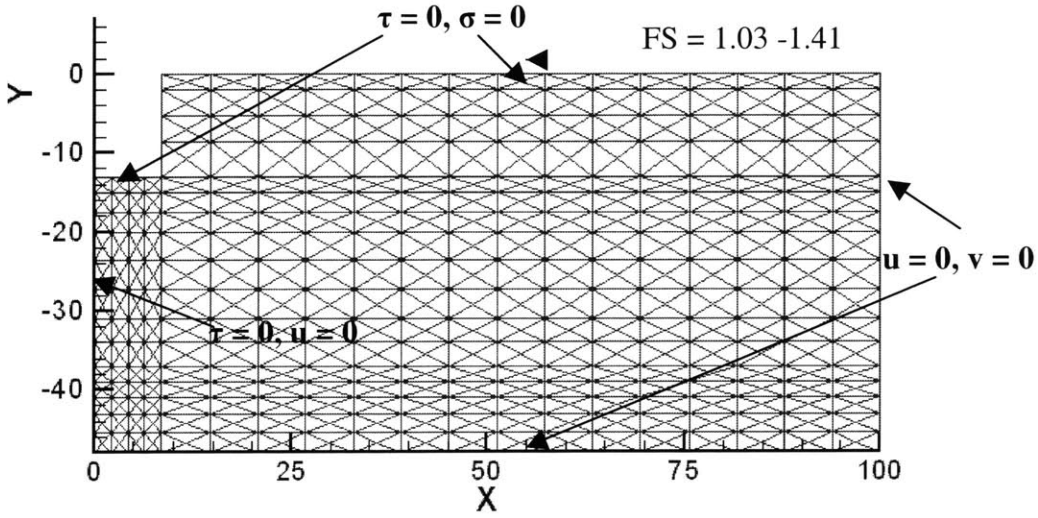

Figure 4.6 Initial Mesh of MMT Excavation Section with Large Overall Dimensions

The upper bound analysis results are shown in Figure 4.7. This figure shows a vector plot of the velocities at failure and the plastic zone (shaded in light gray). The failure zone extends to the base of the Bay Mud and laterally to 40 M from the wall. The light gray zone and vector arrows show the extent and mechanism of failure in the soil mass. Several plastic hinges form in the wall below the lowest level of bracing. For this case, the factor of safety is FS = 1.03-1.41.

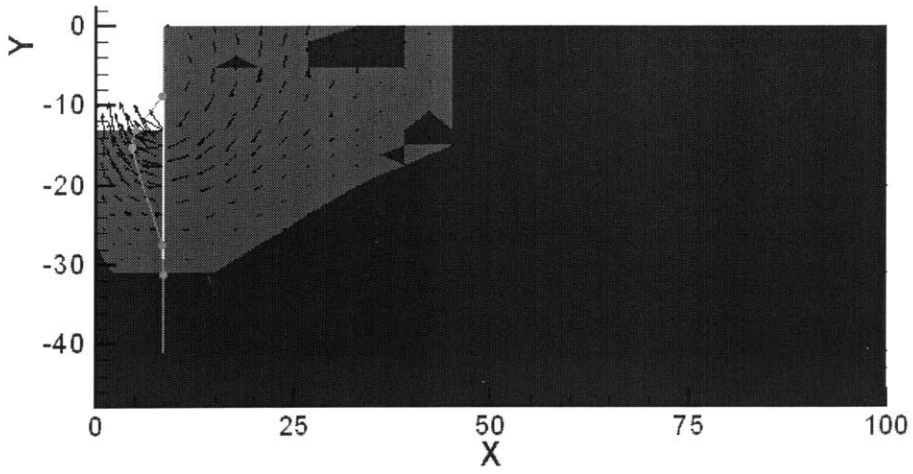

Figure 4.7 Vector Plot and Plastic Zone for Upper Bound Analysis with Initial Mesh

The vertical extent of the plastic zone shown in Figure 4.7 coincides with the deepest plastic hinge observed in the wall at a depth of 31 M, where the Bay Mud ends. Below this depth are stronger layers of sand. Therefore, it is not surprising that the top of the sand layer effectively contains the mechanism. Therefore, we chose to analyze the section contained within a depth of 31 M and 50 M from the centerline of excavation because it contains the entire mechanism. To do this, we must allow for the possibility of a plastic hinge at a depth of 31 M. This was achieved by adding a thin dummy layer of strong soil below the 31 M depth. These dimensions now guarantee that the failure mechanism is completely contained within the mesh, so no error is introduced by reducing the overall dimensions.[10] A similar exercise has also been performed to refine the lower bound analysis.

Now that the boundaries of the section have been determined, the next step is to create a mesh of adequate coarseness. The coarseness the mesh is deemed adequate when refining the mesh further does not significantly improve the results. The author created three meshes of different levels of coarseness and performed analysis on all three meshes to determine the adequate mesh coarseness. Figure 4.8 shows the three meshes that were considered. The first mesh (Figure 4.8a) is a very coarse mesh that was used to obtain a first order approximation of $\bar{\gamma}_l$ and $\bar{\gamma}_u$. The regions contained in this mesh were not subdivided. That is, the horizontal and vertical edges in this mesh define all its regions.

[10] The author verified that after reducing the overall dimensions the answers are still exactly the same.

The second mesh (Figure 4.8b) is defined by the same regions as the first, but the larger regions have been subdivided to achieve relatively uniform element sizes. The third mesh (Figure 4.8c) is also defined by the same regions, but the number of subdivisions was further increased.

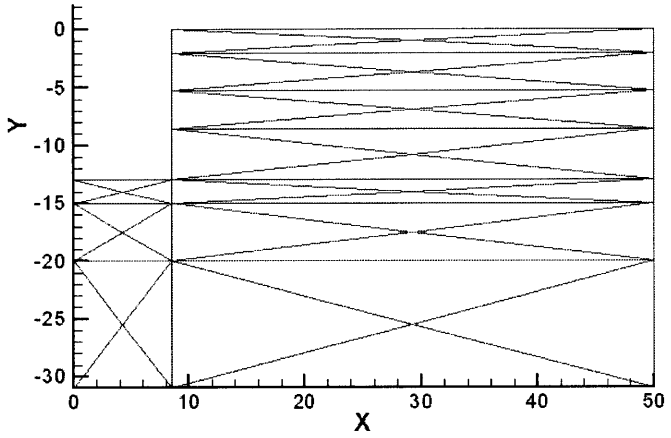

Figure 4.8a Coarse Mesh of Region of Interest

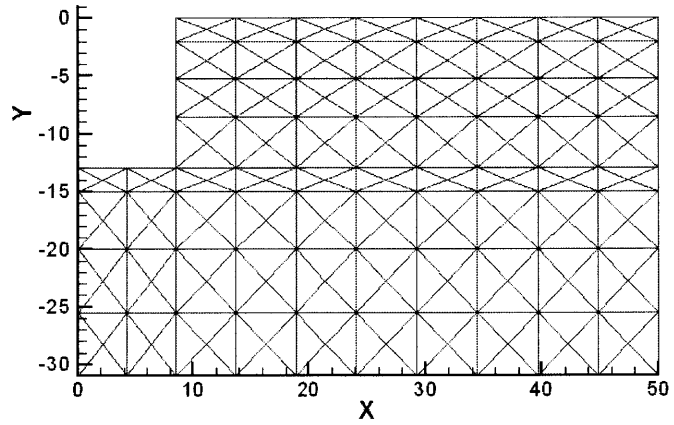

Figure 4.8b Medium Mesh of Region of Interest

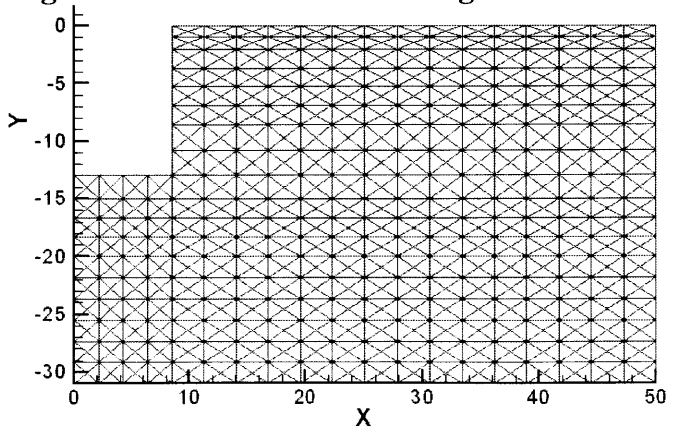

Figure 4.8c Fine Mesh of Region of Interest

Table 4.3 is a summary of the characteristics of the three meshes of Figure 4.8. The table also shows the $\bar{\gamma}_l$ and $\bar{\gamma}_u$ that were found for each mesh and the corresponding computation time. The table clearly shows that the coarse mesh is inadequate since the range defined by $\bar{\gamma}_l$ and $\bar{\gamma}_u$ is unacceptably large. The medium mesh is significantly better since the difference between $\bar{\gamma}_l$ and $\bar{\gamma}_u$ has been reduced by a factor of 4. As we would expect, the fine mesh gives the best set of results. This mesh is about four times finer than the medium mesh, but the difference between $\bar{\gamma}_l$ and $\bar{\gamma}_u$ is only reduced by 25% relative to the medium mesh. At the same time, computation time has also increased dramatically. Computation time is not proportional to the number of nodes or elements in the mesh. In fact, computation time increases at increasing rates as meshes get finer. Therefore, it is clear that the precision of the results for each mesh is subject to diminishing rates of return as mesh fineness increases. At this point, the author decided that the benefits of the small increase in precision do not justify using finer meshes due to the loss of time. The fine mesh is used for the remaining analysis of the MMT case study.

Mesh	Number of Nodes	Number of Elements	$\bar{\gamma}_l$ (kN/m^3)	$\bar{\gamma}_u$ (kN/m^3)	Computation Time
Coarse	144	48	13.64	38.42	1 seconds
Medium	1104	368	16.94	22.98	1.5 minutes
Fine	4176	1492	17.41	22.27	63 minutes

Table 4.3 Effect of Mesh Refinement on Stability Calculations by Numerical Limits

4.4.2 Analysis of Results

Figure 4.9 summarizes the results of the lower bound analysis for the MMT. Figures 4.9a and 4.9b show contours of the major and minor principal stresses respectively. As we would expect, the principal stresses both increase with depth and their contours follow similar patterns.

Figure 4.9c shows contours of the direction of the major principal stress measured by the angle, δ, to the vertical. This figure shows that δ rotates about the bottom level of bracing. Near the bottom of the retained soil, it reaches a minimum between 0 and 6°, and then increases as it rotates into the excavation. The maximum recorded value of δ is 90°, which occurs inside the excavation as we expect since this zone fails in extension.

Figure 4.10 shows the results of the upper bound analysis. Figure 4.10a shows the deformed mesh at failure and the deflections of the wall. This figure shows the general pattern of movement during collapse. The wall develops four plastic in this refined mesh (instead of 5 hinges in Figure 4.7). Furthermore, there is no longer a plastic hinge at a depth of 31 M in this mechanism, which is also a result of the different mesh arrangement.

Figure 4.10b shows a vector plot and the plastic zone in the area of interest during collapse. The deflections of the wall are also included for completeness. As predicted, the plastic zone is completely contained within the clay. In fact, the plastic zone does not extend to the bottom of the clay as Figure 4.7 suggested. Again, this failure mechanism is lightly different than the one shown in Figure 4.6 due to the different mesh arrangement, which is why the location of the plastic zone is different. We also note that the lateral boundary extends well beyond the plastic zone, so boundary effects are effectively eliminated from the analysis.

The vector plot agrees with the deformation pattern shown by the deformed mesh. Both figures show that at failure, the top of the retained soil subsides. This movement pushes the wall into the excavation and causes the plastic hinges observed in the wall. The movement of the wall then causes heave inside the excavation (due to the constraint of zero horizontal velocity inside the excavation).

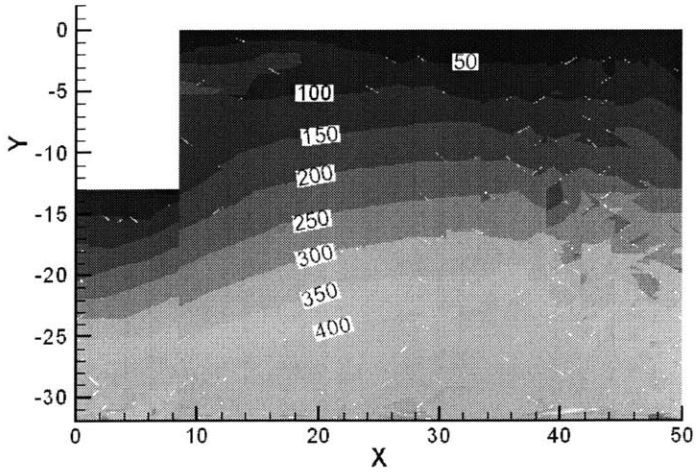

Figure 4.9a Contours of σ_1 in Area of Interest

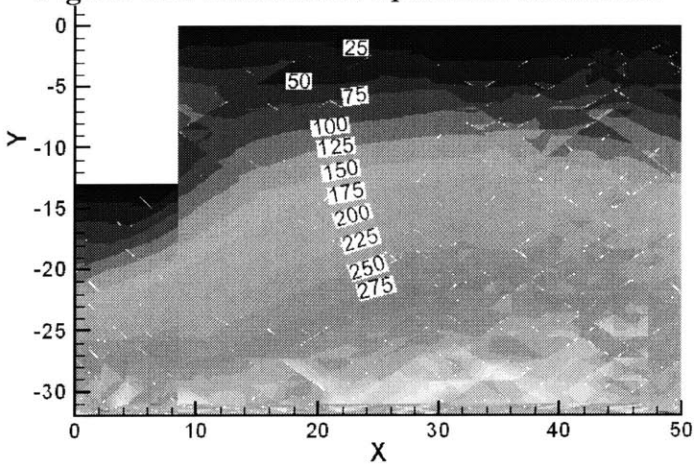

Figure 4.9b Contours of σ_3 in Area of Interest

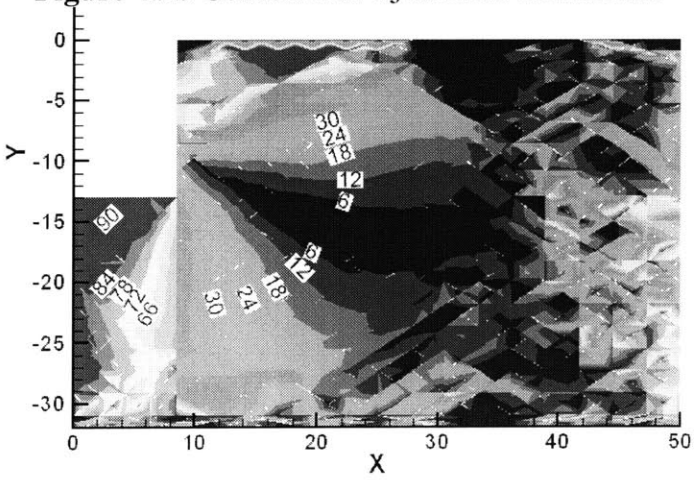

Figure 4.9c Contours of δ in Area of Interest

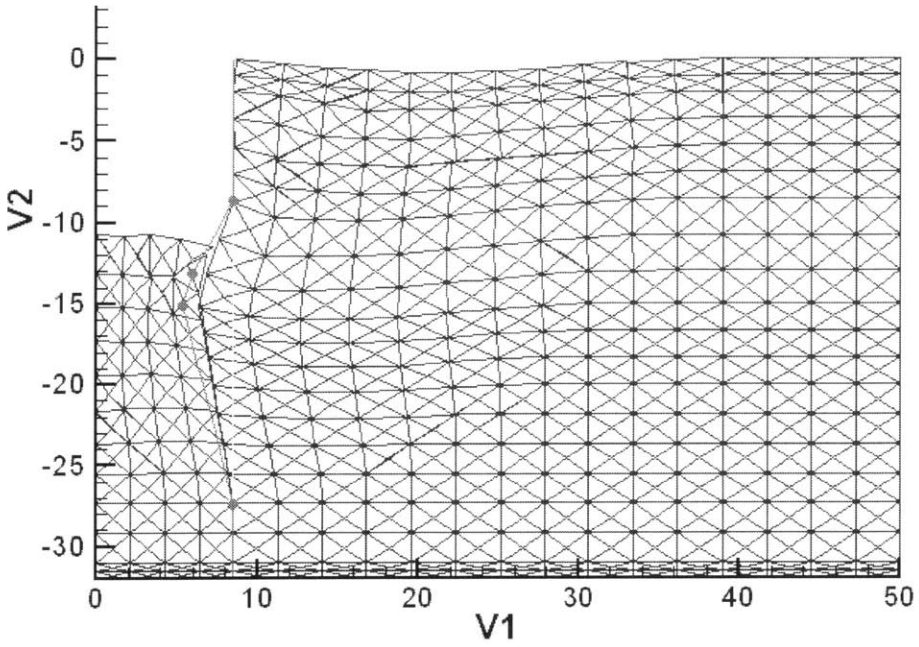

Figure 4.10a Deformed Mesh of Area of Interest

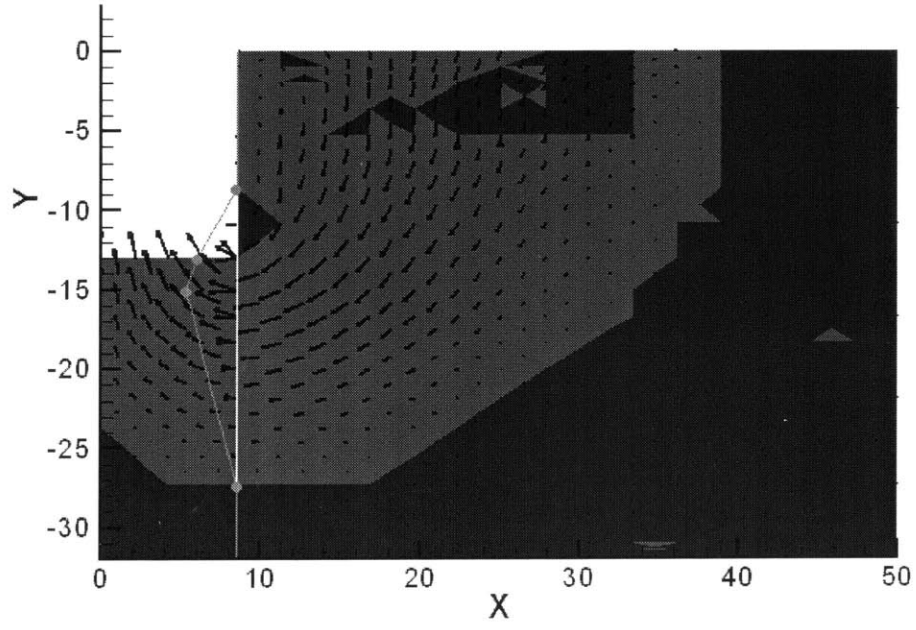

Figure 4.10b Vector Plot and Plastic Zone of Area of Interest

In excavations the factor of safety is defined as the ratio of the vertical stress caused by the retained soil at failure to the vertical stress caused by the retained soil in situ. That is,

$$FS = \frac{\sum(\gamma_i B_i)_{failure}}{\sum(\gamma_i B_i)_{insitu}}. \quad (4.1)$$

Since both limit theorems provide bounds on the failure conditions, we can bound the actual *FS* according to

$$\frac{\sum(\gamma_i B_i)_l}{\sum(\gamma_i B_i)_{insitu}} \leq FS \leq \frac{\sum(\gamma_i B_i)_u}{\sum(\gamma_i B_i)_{insitu}}. \quad (4.2)$$

These calculations were performed and the results are tabulated on Table 4.4. Therefore, we can conclude that the factor of safety *must* be between *FS*=1.032-1.362. Alternatively, we can guarantee *FS* =1.197 ±13.8%.

	Lower Bound	**Upper Bound**	**Average**
$\gamma_{optimum}$ **(kN/m^3)**	17.41	22.27	19.84
FOS	1.032	1. 362	1.197

Table 4.4 Tabulation of FOS Range for MUNI Metro Turnback Project

Koutsoftas et al. (2000) evaluates the *FS* of this section using the limit equilibrium method developed by Eide et al. (1972). They calculate a factor of safety of 1.2, which is in the range we derived through limit theorems.[11] By using limit theorems we can therefore guarantee that the factor of safety calculated in Koutsoftas et al. (2000) accurate within 13.8%.

Figure 4.11 compares the *FS* calculated by Koutsoftas et al. (2000) to those calculated using numerical limit analysis. The figure shows that *FS* estimates of upper bound analysis closely matched those reported in Koutsoftas et al. (2000). However the lower bound analysis gives significantly smaller estimates of *FS*.

Limit theorems offer a certainty range on *FS*, which allows the engineer to evaluate the precision of the *FS* estimate. This is one advantage that the numerical limit analysis has over limit equilibrium methods. The range in *FS* computed for this case study, however, is larger than that found by Ukritchon (1998) for similar excavation

[11] The author performed an independent check on the factor of safety using the method recommended by Eide et al. (1972) and determined that *FS* = 1.2 is a reasonable estimate if the length of the piles beyond the concreted portion of the wall is ignored.

problems. The principal reason is almost certainly liked to the relatively crude meshes used in the lower bound analysis of the MMT project.

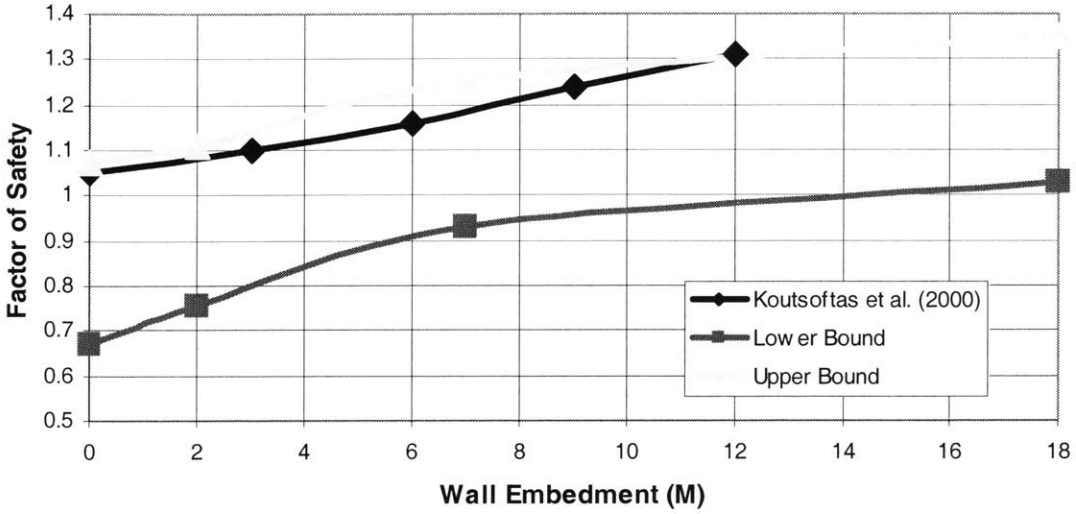

Figure 4.11 Comparison of *FS* Calculated by Koutsoftas et al. (2000) Vs. Numerical Limit Analysis

Chapter 5. Conclusions and Recommendations

5.1 MMT Case Study

We were able to reproduce and validate the *FS* estimates reported in Koutsoftas et al. (2000) for the 13 M deep excavation in the test section of the MMT project by using numerical limit analysis. Koutsoftas et al. (2000) reports a $FS = 1.2$ for this section while we calculated $FS = 1.03\text{-}1.36$. Therefore we conclude that $FS = 1.2$ is a reasonable estimate of the factor of safety for this section of the excavation.

Ideally, the lower bound analysis should be repeated using more sophisticated, non-uniform meshes to get more accurate lower bound results. It is likely that this will greatly reduce the difference between the lower and upper bound estimates of *FS*, and it will probably show conclusively that the limit equilibrium method used to evaluate instability of the MMT excavations by Koutsoftas et al. (2000) gives conservative estimates of *FS* for this case study.

We were also able to produce estimates of stresses at failure and predict the failure mechanism by using numerical limit analysis. These results allow us to analyze the behavior of the excavation at failure without the need to consider stress-stain-strength relationships.

5.2 Limit Theorems and their Numerical Formulations

The benefits of limit theorems are evident. Their simplicity and adaptability to computer algorithms allows engineers to estimate collapse loads relatively quickly by bounding actual solutions. By incremental adjustments to the meshes, the difference between lower and upper bound estimates can be reduced to a manageable range. As a result, the engineer can usually *guarantee* that his estimate of the solution is within 5% of the actual solution. This is a remarkable result that is very difficult to accomplish by any other means.

The only disadvantage of the limit theorems themselves is the need to assume $\psi=\phi$ (Equation 2.13) in Mohr-Coulomb materials to ensure the integrity of the lower bound theorem. As we have mentioned, this assumption generally does not hold for

drained materials and as a consequence, the lower bound theorem has theoretical limitations in simulating the real drained shear strength of soils that require non-associated flow conditions.

Although each program that was used to apply limit theorems fulfills its purpose, each has disadvantages that are common in software in this stage of development. The most evident problem, which unfortunately refers to all the programs discussed in Chapter 3, is the lack of a graphical user interface (GUI). The lack of a GUI has two major effects on the analysis process. First, it means all the required inputs have to be input manually into text files. This is not a major limitation for simple problems, but for more complex problems this implies the need to manually change inputs in hundreds of pages of text. Second, the lack of a GUI means new users must invest a significant amount of time to learn how to use all the programs before they can apply this method of analysis to case studies.

Another related disadvantage that plagues all the programs is the lack of error traps. Small mistakes in the input files can lead to large errors, and the programs should have more error traps to locate common mistakes. A good example of a mistake that can easily be avoided by creating an error trap occurs in the mesh generators. LBmain and UBmain require all nodes that are not on a boundary to have other nodes at the same location. That is, LBmain and UBmain do not allow "floating points" between soil elements. A problem arises because LBgen and UBgen create floating points between elements if the user inputs the mesh data incorrectly. This can easily be avoided by having the program verify that all regions that are horizontally and vertically adjacent have the same number of subdivisions in the y and x directions respectively. There are many other simple error traps that can be introduced that will reduce the possibility of error from inadequate input.

The author believes limit theorems and their applications in geotechnical engineering are very useful tools. Moreover, we are almost at a point where their power in determining collapse loads has reached full capacity since we can usually estimate collapse loads within 5%. If the use of limit theorems embedded in linear programming software became widespread, the result would be a significant improvement in excavation design. However, before this occurs the software must all be unified behind a

single GUI that makes using these tools easier. The program should be able to handle mesh generation and optimization simultaneously, and there should be adequate error traps that identify common errors.

List of References

Atkinson, J.H., Bransby, P.L. (1978). The Mechanics of Soils, an Introduction to Critical State Soil Mechanics, McGraw-Hill.

Drucker, D.C., Greenberg, H.J. and Prager, W. (1952). "Extended Limit Design Theorems for Continuous Media." Q. Appl. Math., 9, pp. 381-389

Eide, O., Aas, G., Josang, T. (1972) "Special Application of Cast-in-Place Walls for Tunnels in Soft Clay in Oslo." *Proc. 5th European Conference on Soil Mechanics and Foundation Engineering*. Spanish Society of Soil Mechanics and Foundations. Madrid, Spain, pp. 485-498

Koutsoftas, D., Frobenius, P., Wu, C., Meyersohn, D., Kulesza, R. (2000) "Deformations During Cut-and-Cover Construction of MUNI Metro Turnback Project." *ASCE Journal of Geotechnical and Geoenvironmental Engineering*. Vol. 126, No. 4, pp. 344-359

Ladd. C. C., Foot, R. (1974). "New Design Procedure for Stability of Soft Clays." *ASCE Journal of Geotechnical and Geoenvironmental Engineering*. Vol. 100, No. 7, pp. 763-786

O'Rourke, T.D., O'Donnell, C.J. (1997). "Field Behavior of Excavation Stabilized by Deep Soil Mixing." *ASCE Journal of Geotechnical and Geoenvironmental Engineering*. Vol. 123, No. 6, pp. 516-524

O'Rourke, T.D., O'Donnell, C.J. (1997). "Deep Rotational Stability of Tiedback Excavations in Clay." *Journal of Geotechnical and Geoenvironmental Engineering*. Vol. 123, No. 6, pp. 506-515

O'Rourke, T.D. (1993). Retaining Structures. "Base Stability and Ground Movement Prediction for Excavations in Soft Clay." *Institution of Civil Engineers*. Thomas Telford; London

Prasad, A. (2003). "Development of a User Interface for Numerical Limit Analysis of Geotechnical Stability Problems." M.S. Thesis, Department of Civil and Environmental Engineering, Massachusetts Institute of Technology, Cambridge MA

Sloan, S.W., Kleeman, P.W. (1995) "Upper Bound Limit Analysis Using Discontinuous Velocity Fields." *Computer Methods in Applied Mechanics and Engineering*, No. 127, pp. 293-314

Sloan S.W. (1988). "Lower Bound Limit Analysis Using Finite Elements and Linear Programming." *International Journal for Numerical and Analytical Methods in Geomechanics*. Vol. 12, No. 1, pp 21-77

Ukritchon, B. (1996). "Evaluation of Numerical Limit Analysis by Finite Elements and Linear Programming." M.S. Thesis, Department of Civil and Environmental Engineering, Massachusetts Institute of Technology, Cambridge MA

Ukritchon, B. (1998). "Application of Numerical Limit Analysis for Undrained Stability Problems in Clay." Sc.D. Thesis, Department of Civil and Environmental Engineering, Massachusetts Institute of Technology, Cambridge MA

Ukritchon, B., Whittle, A.J. & Sloan, S.W. (2003) "Undrained Stability of braced Excavations in clay," *ASCE Journal of Geotechnical and Geoenvironmental Engineering*, Vol. 129, No. 8, 738-756.

Appendix A. Sample Input File for LBgen

```
23              , total number of points defined
12              , total number of regions defined by points
0               , nsel (not required here)
0               , transition zone (not required here)
3               , number of boundary edges (where boundary conditions will be defined)
0               , extension zone (not required here)
6               , number of layers
4               , number of beam segment that define the beam element
1  0.0  -32     , syntax for nodes is (node number / x coordinate / y coordinate)
2  0.0  -31
3  0.0  -20
4  0.0  -15
5  0.0  -13
6  8.5  -32
7  8.5  -31
8  8.5  -20
9  8.5  -15
10 8.5  -13
11 8.5  -8.6
12 8.5  -5.3
13 8.5  -2
14 8.5   0.0
15 50   -32
16 50   -31
17 50   -20
18 50   -15
19 50   -13
20 50   -8.6
21 50   -5.3
22 50   -2
23 50    0.0
1  1   1   7   4  2    , Syntax for regions is (region number / region shape
2  1   6   16   15 2   , [1 is rectangle] / Lower left node [for shape 1 region] /
3  1   2   8   4  6    , Upper right node [for shape 1 region] / Number of subdivisions
4  1   7   17   15 6   , in x direction / Number of subdivisions in y direction)
5  1   3   9   4  3
6  1   8   18   15 3
7  1   4   10   4  1
8  1   9   19   15 1
9  1   10  20   15 2
10 1   11  21   15 2
11 1   12  22   15 2
12 1   13  23   15 2
```

```
1 1   5          , Syntax for boundary edge data is (boundary edge number / node
2 5   10         , on one end of boundary edge / node on other end of boundary
3 14  23         , edge)
1 0.0 -2         , syntax for layer data is (layer number / elevation of top of layer /
2 -2  -5.3       , elevation of bottom of layer)
3 -5.3 -13
4 -13  -15
5 -15  -31
6 -31  -37
1 6   11         , syntax for beam segment data is (segment number / node on one
2 11  12         , end of beam segment / node on other end of beam segment)
3 12  13
4 13  14
```

Appendix B. Sample Input File for LBmain

1 F T T F
Print (int), mesh generation(T/F), Scale(T/F) , Steep(T/F), store (T/F)
4176 1 1392 0 0 2037 2 6 1
Soil Summary;
Number of: nodes, unique coordinates, triangular elements, triangular extension, rectangular extension, number of discontinuities, unit weights, material no, water tables
40 20 18 3 1
Beam Summary;
Number of : nodes, beam elements, joint element, support, material no
1 -1
2 1
Unit Weights;
Reference unit weight number, unit weight (negative unit weight indicates unit weight will be optimized)
1
Factor of safety
1 1
.000 0.0 0.0 30 1 24
2 3
-2.000 0.0 0.0 30 1 1 24
3 1
-5.300 20 1.375 0.0 1 24
4 1
-5.300 20 1.375 0.0 2 24
5 1
-15.000 33.375 2.503 0.0 2 24
6 1
-31.000 0.0 0.0 30 2 24.
Soil Material Properties;
Line 1: Material reference number, soil type
Line 2:
Soil type 1 indicates total stress analysis;
reference elevation, S_u at reference elevation, gradient of S_u, friction angle, reference unit weight number, p (number of linear segments approximating failure criterion)
Soil type 2 is anisotropic soil, which is not discussed here
If soil type 3 indicates effective stress analysis;
reference elevation, S_u at reference elevation, gradient of S_u, friction angle, reference unit weight number, reference water table, p (number of linear segments approximating failure criterion)
1 1
-2 9.81
Water Table Properties;
Line 1: Reference water table number, water table type

Line 2:

Type 1 water table indicates hydrostatic pore pressures;

elevation of water tale, unit weight of water

Type 2 water table indicates pore pressures proportional to overburden

Number of nodes defining water table (m)

m lines containing two nodes each to define segments of water table

Proportion of overburden stress that is pore pressure

1 1

882

Beam Material Properties;

Line 1: Beam material reference number, beam material type

Line 2:

Type one indicates only limited moment capacity

Moment capacity

4 other types are not discussed here

1	1.06250000000000	-31.75000000000000
2	.00000000000000	-32.00000000000000
3	2.12500000000000	-32.00000000000000
4	1.06250000000000	-31.75000000000000
4213	8.50000000000000	-2.00000000000000
4214	8.50000000000000	-1.00000000000000
4215	8.50000000000000	-1.00000000000000
4216	8.50000000000000	.00000000000000

Node coordinate information (only beginning and end);

Node number, x coordinate, y coordinate

3450	2
3451	2
3452	2
3453	2
3454	2
3455	2
3456	2
3457	2
3458	2
3459	2
3460	2
3461	2
3462	2
3463	2
3464	2
3465	2
3466	1
3467	2
3468	2
3469	2
3470	1

Joint Information (complete)
Joint number, nodes defining joint (joints at ends of beam segments only have 1 joint)

1	1	2	3	6
2	4	5	6	6
3	7	8	9	6
4	10	11	12	6
5	13	14	15	6
6	16	17	18	6
1383	4147	4148	4149	1
1384	4150	4151	4152	1
1385	4153	4154	4155	1
1386	4156	4157	4158	1
1387	4159	4160	4161	1
1388	4162	4163	4164	1
1389	4165	4166	4167	1
1390	4168	4169	4170	1
1391	4171	4172	4173	1
1392	4174	4175	4176	1

Triangular element information (only beginning and end);
Element number, 1st node in element, 2nd node in element, 3rd node in element, soil material reference number

1393	10	1	12	2	0
1394	5	3	4	1	0
1395	24	5	23	6	0
1396	8	6	7	4	0
1397	51	8	50	9	0
1398	11	9	10	7	0
1399	22	13	24	14	0
3421	4162	4153	4164	4154	0
3422	4157	4155	4156	4153	0
3423	4176	4157	4175	4158	0
3424	4160	4158	4159	4156	0
3425	4163	4161	4162	4159	0
3426	4174	4165	4176	4166	0
3427	4169	4167	4168	4165	0
3428	4172	4170	4171	4168	0
3429	4175	4173	4174	4171	0

Discontinuity information (only beginning and end);
Discontinuity number, 1st node in element, 2nd node in element, 3rd node in element,4th node in element, soil material reference number (always zero for discontinuities)

3430	4177	4178	1
3431	4179	4180	1
3432	4181	4182	1
3433	4183	4184	1
3434	4185	4186	1
3435	4187	4188	1

3436 4189 4190 1
3437 4191 4192 1
3438 4193 4194 1
3439 4195 4196 1
3440 4197 4198 1
3441 4199 4200 1
3442 4201 4202 1
3443 4203 4204 1
3444 4205 4206 1
3445 4207 4208 1
3446 4209 4210 1
3447 4211 4212 1
3448 4213 4214 1
3449 4215 4216 1

Beam element information (complete);
Beam element number, node on one end of beam segment, node on other end of beam segment, beam material reference number

3450 4178 4179
3451 4180 4181
3452 4182 4183
3453 4184 4185
3454 4186 4187
3455 4188 4189
3456 4190 4191
3457 4192 4193
3458 4194 4195
3459 4196 4197
3460 4198 4199
3461 4200 4201
3462 4202 4203
3463 4206 4207
3464 4210 4211
3465 4214 4215
3466 4177
3467 4204 4205
3468 4208 4209
3469 4212 4213
3470 4216

Joint information;
Joint number, nodes defining joint

3

number of boundary conditions

24

12 11 60 59 468 467 516 515 564 563 612 611

660 659 708 707 1836 1835 1884 1883

1932 1931 2520 2519
CON NONE
T
0.0 F
8
2517 2516 2529 2528 2541 2540 2553 2552
CON CON
T
0.0 F
T
0.0 F
30
4005 4004 4017 4016 4029 4028 4041 4040 4053 4052 4065 4064

4077 4076 4089 4088 4101 4100 4113 4112
4125 4124 4137 4136 4149 4148 4161 4160 4173 4172
CON CON
T
0.0 F
T
0.0 F
Boundary condition information for boundary edges
Line 1: Number of nodes on boundary
Line 2: Nodes on boundary
Line 3: Type of boundary condition
Shear boundary condition, normal boundary condition
NONE indicates no constraint along boundary
No information required
CON indicates constant stress along boundary
Flag (T indicates value will be prescribed, F indicates otherwise)
Value of boundary stress, Flag to apply factor of safety (F for no)
LIN indicates linear variation along boundary
Not discussed here
0
point loads (not used and not discussed)
0
int shear (not used and not discussed)
0
print out for nor,tau (not used and not discussed)
1
3
3467 3468 3469
F T T
0.0d0 F
0.0d0 F
Support boundary conditions;

Line 1: Number of joints
Line 2: Joint Numbers
Line 3: Flags shear, vertical, and moment support
Line 4: Values of boundary condition, Flag to apply factor of safety
0
applied force at joint (not used and not discussed)

0 , distributed load for beams *(not used and not discussed)*
20
Number of soil-structure interfaces
3430
 108 107 41 42
F
3431
 288 287 89 90
F
3432
 756 755 497 498
F
3433
 936 935 545 546
F
3434
 1116 1115 593 594
F
3435
 1296 1295 641 642
F
3436
 1476 1475 689 690
F
3437
 1656 1655 737 738
F
3438
 1980 1979 1865 1866
F
3439
 2160 2159 1913 1914
F
3440
 2340 2339 1961 1962
F
3441
 2568 2567 2549 2550
F

3442
2748 2747 0 0
F
3443
2928 2927 0 0
F
3444
3108 3107 0 0
F
3445
3288 3287 0 0
F
3446
3468 3467 0 0
F
3447
3648 3647 0 0
F
3448
3828 3827 0 0
F
3449
4008 4007 0 0
F

Soil structure interaction;
Line 1: Beam element number
Line 2: Nodes defining interface
Line 3: Flag for prescribed boundary condition on interface
Line 4: Value of interface stress, Flag to apply factor of safety

Appendix C. Sample Input File for UBgen

```
23              , total number of points defined
12              , total number of regions defined by points
0               , nsel (not required here)
3               , number of boundary edges (where boundary conditions will be defined)
0               , number of loads (not required here)
6               , number of layers
4               , number of beam segment that define the beam element
1  0.0  -32     , syntax for nodes is (node number / x coordinate / y coordinate)
2  0.0  -31
3  0.0  -20
4  0.0  -15
5  0.0  -13
6  8.5  -32
7  8.5  -31
8  8.5  -20
9  8.5  -15
10 8.5  -13
11 8.5  -8.6
12 8.5  -5.3
13 8.5  -2
14 8.5   0.0
15 50   -32
16 50   -31
17 50   -20
18 50   -15
19 50   -13
20 50   -8.6
21 50   -5.3
22 50   -2
23 50    0.0
1  1   1   7   4  2     , Syntax for regions is (region number / region shape
2  1   6   16  15 2     , [1 is rectangle] / Lower left node [for shape 1 region] /
3  1   2   8   4  6     , Upper right node [for shape 1 region] / Number of subdivisions
4  1   7   17  15 6     , in x direction / Number of subdivisions in y direction)
5  1   3   9   4  3
6  1   8   18  15 3
7  1   4   10  4  1
8  1   9   19  15 1
9  1   10  20  15 2
10 1   11  21  15 2
11 1   12  22  15 2
12 1   13  23  15 2
1  5   1               , Syntax for boundary edge data is (boundary edge number / node
```

```
2 1   15          , on one end of boundary edge / node on other end of boundary
3 15  23          , edge)
1 0.0 -2          , syntax for layer data is (layer number / elevation of top of layer /
2 -2  -5.3        , elevation of bottom of layer)
3 -5.3 -13
4 -13  -15
5 -15  -31
6 -31  -37
1 6   11          , syntax for beam segment data is (segment number / node on one
2 11  12          , end of beam segment / node on other end of beam segment)
3 12  13
4 13  14
```

Appendix D. Sample Input File for UBmain

1 F T T F
Print (int), mesh generation(T/F), Scale(T/F) , Steep(T/F), store (T/F)
4176 1 1392 2069 2 6 1
Soil Summary;
Number of: nodes, unique coordinates, triangular elements, discontinuities, unit weights, material numbers, water tables
40 20 21 1
Beam Summary;
Number of : nodes, beam elements, joint element, material no
1 -1
2 1
Unit Weights;
Reference unit weight number, unit weight (negative unit weight indicates unit weight will be optimized)
1
Factor of safety
1 1
.000 0.0 0.0 30 1 24
2 3
-2.000 0.0 0.0 30 1 1 24
3 1
-5.300 20 1.375 0.0 1 24
4 1
-5.300 20 1.375 0.0 2 24
5 1
-15.000 33.375 2.503 0.0 2 24
6 1
-31.000 0.0 0.0 30 2 24.
Soil Material Properties;
Line 1: Material reference number, soil type
Line 2:
Soil type 1 indicates total stress analysis;
reference elevation, S_u at reference elevation, gradient of S_u, friction angle, reference unit weight number, p (number of linear segments approximating failure criterion)
Soil type 2 is anisotropic soil, which is not discussed here
If soil type 3 indicates effective stress analysis;
reference elevation, S_u at reference elevation, gradient of S_u, friction angle, reference unit weight number, reference water table, p (number of linear segments approximating failure criterion)
1 1
-2 9.81
Water Table Properties;
Line 1: Reference water table number, water table type

Line 2:

Type 1 water table indicates hydrostatic pore pressures;
elevation of water tale, unit weight of water
Type 2 water table indicates pore pressures proportional to overburden
Number of nodes defining water table (m)
m lines containing two nodes each to define segments of water table
Proportion of overburden stress that is pore pressure

1 1
882
Beam Material Properties;
Line 1: Beam material reference number, beam material type
Line 2:

Type one indicates only limited moment capacity
Moment capacity
4 other types are not discussed here

1	1.06250000000000	-31.75000000000000
2	.00000000000000	-32.00000000000000
3	2.12500000000000	-32.00000000000000
4	1.06250000000000	-31.75000000000000
4213	8.50000000000000	-2.00000000000000
4214	8.50000000000000	-1.00000000000000
4215	8.50000000000000	-1.00000000000000
4216	8.50000000000000	.00000000000000

Node coordinate information (only beginning and end);
Node number, x coordinate, y coordinate

3450	2
3451	2
3452	2
3453	2
3454	2
3455	2
3456	2
3457	2
3458	2
3459	2
3460	2
3461	2
3462	2
3463	2
3464	2
3465	2
3466	1
3467	2
3468	2
3469	2
3470	1

Joint Information (complete)
Joint number, nodes defining joint (joints at ends of beam segments only have 1 joint)

1	1	2	3	6
2	4	5	6	6
3	7	8	9	6
4	10	11	12	6
5	13	14	15	6
6	16	17	18	6
1383	4147	4148	4149	1
1384	4150	4151	4152	1
1385	4153	4154	4155	1
1386	4156	4157	4158	1
1387	4159	4160	4161	1
1388	4162	4163	4164	1
1389	4165	4166	4167	1
1390	4168	4169	4170	1
1391	4171	4172	4173	1
1392	4174	4175	4176	1

Triangular element information (only beginning and end);
Element number, 1st node in element, 2nd node in element, 3rd node in element, soil material reference number

1393	10	1	12	2	0
1394	5	3	4	1	0
1395	24	5	23	6	0
1396	8	6	7	4	0
1397	51	8	50	9	0
1398	11	9	10	7	0
1399	22	13	24	14	0
3421	4162	4153	4164	4154	0
3422	4157	4155	4156	4153	0
3423	4176	4157	4175	4158	0
3424	4160	4158	4159	4156	0
3425	4163	4161	4162	4159	0
3426	4174	4165	4176	4166	0
3427	4169	4167	4168	4165	0
3428	4172	4170	4171	4168	0
3429	4175	4173	4174	4171	0

Discontinuity information (only beginning and end);
Discontinuity number, 1st node in element, 2nd node in element, 3rd node in element,4th node in element, soil material reference number (always zero for discontinuities)

3430	4177	4178	1
3431	4179	4180	1
3432	4181	4182	1
3433	4183	4184	1
3434	4185	4186	1
3435	4187	4188	1

3436 4189 4190 1
3437 4191 4192 1
3438 4193 4194 1
3439 4195 4196 1
3440 4197 4198 1
3441 4199 4200 1
3442 4201 4202 1
3443 4203 4204 1
3444 4205 4206 1
3445 4207 4208 1
3446 4209 4210 1
3447 4211 4212 1
3448 4213 4214 1
3449 4215 4216 1

Beam element information (complete);
Beam element number, node on one end of beam segment, node on other end of beam segment, beam material reference number

3450 4178 4179
3451 4180 4181
3452 4182 4183
3453 4184 4185
3454 4186 4187
3455 4188 4189
3456 4190 4191
3457 4192 4193
3458 4194 4195
3459 4196 4197
3460 4198 4199
3461 4200 4201
3462 4202 4203
3463 4206 4207
3464 4210 4211
3465 4214 4215
3466 4177
3467 4204 4205
3468 4208 4209
3469 4212 4213
3470 4216

Joint information;
Joint number, nodes defining joint

3

number of boundary conditions

24

2519 2520 1931 1932 1883 1884 1835 1836 707 708 659 660 611 612 563 564 515 516 467 468 59 60 11 12

T F

.00 .00 .00 .00 .00 .00 .00 .00 .00 .00 .00 .00 .00 .00 .00 .00 .00 .00 .00 .00
.00 .00 .00 .00
38
2 3 14 15 26 27 38 39 98 99 110 111 122 123 134 135 146 147 158
159 170 171 182 183 194 195 206 207 218 219 230 231 242 243 254 255 266
267
T T
.00 .00 .00 .00 .00 .00 .00 .00 .00 .00 .00 .00 .00 .00 .00 .00 .00 .00 .00 .00
.00 .00 .00 .00 .00 .00 .00 .00 .00 .00 .00 .00 .00 .00 .00 .00 .00 .00
.00 .00 .00 .00 .00 .00 .00 .00 .00 .00 .00 .00 .00 .00 .00 .00 .00 .00 .00 .00
.00 .00 .00 .00 .00 .00 .00 .00 .00 .00 .00 .00 .00 .00 .00 .00 .00 .00
40
269 270 449 450 917 918 1097 1098 1277 1278 1457 1458 1637 1638 1817 1818
2141 2142 2321 2322 2501 2502 2729 2730 2909 2910 3089 3090 3269 3270 3449 3450
3629 3630 3809 3810 3989 3990 4169 4170
T T
.00 .00 .00 .00 .00 .00 .00 .00 .00 .00 .00 .00 .00 .00 .00 .00 .00 .00 .00 .00
.00 .00 .00 .00 .00 .00 .00 .00 .00 .00 .00 .00 .00 .00 .00 .00 .00 .00 .00 .00
.00 .00 .00 .00 .00 .00 .00 .00 .00 .00 .00 .00 .00 .00 .00 .00 .00 .00 .00 .00
.00 .00 .00 .00 .00 .00 .00 .00 .00 .00 .00 .00 .00 .00 .00 .00 .00 .00 .00 .00

Boundary condition information for boundary edges
Line 1: Number of nodes on boundary
Line 2: Nodes on boundary
Line 3: Type of boundary condition
Tangential velocity boundary condition flag, normal velocity boundary condition flag (T if value prescribed, F if unconstrained)
Value of velocity boundary condition, Flag to apply factor of safety

0
distributed stress on boundary (not used and not discussed)

0
point loads (not used and not discussed)

1 ,vel bcs of joint
3 ,#of joints
3499 3500 3501
T F F
0.0

Boundary conditions on joints
Line 1: Number of joints
Line 2: Joint Numbers
Line 3: Flags for constraints in x, y, and z directions
Line 4: Values of boundary condition

0
applied forces at joint (not used and not discussed)

0
applied stress for beams(not used and not discussed)